Noname manuscript No.
(will be inserted by the editor)

Human multi-robot physical interaction: a distributed framework

Martina Lippi · Alessandro Marino

the date of receipt and acceptance should be inserted later

Abstract The objective of this paper is to devise a general framework to allow a human operator to physically interact with an object manipulated by a multi-manipulator system in a distributed setting. A two layer solution is devised. In detail, at the top layer an arbitrary virtual dynamics is considered for the object with the virtual input chosen as the solution of an optimal Linear Quadratic Tracking (LQT) problem where both the human and robots' intentions are taken into account, being the former online estimated by Recursive Least Squares (RLS) technique. The output of this layer is a desired trajectory of the object which is the input of the bottom layer and from which desired trajectories for the robot end effectors are computed based on the closed-chain constraints. Each robot, then, implements a time-varying gain adaptive control law so as to take into account model uncertainty and internal wrenches that inevitably raise due to synchronization errors and dynamic and kinematic uncertainties. Remarkably, the overall solution is devised in a distributed setting by resorting to a leader-follower approach and distributed observers. Simulations with 3 6-DOFs serial chain manipulators mounted on mobile platforms corroborate the theoretical findings.

Martina Lippi
Università degli Studi di Salerno, Via Giovanni Paolo II, 132, 84084, Fisciano (SA), Italy
E-mail: mlippi@unisa.it

Alessandro Marino
Università degli Studi di Cassino e del Lazio Meridionale, Via Di Biasio, 43, 03043, Cassino (FR), Italy
E-mail: {al.marino}@unicas.it

* This work is supported by Dipartimento di Eccellenza granted to DIEI Department, University of Cassino and Southern Lazio and by H2020-ICT project CANOPIES-A Collaborative Paradigm for Human Workers and Multi-Robot Teams in Precision Agriculture Systems (Grant Agreement N. 101016906).
· Journal of Intelligent and Robotic Systems
· https://doi.org/10.1007/s10846-020-01277-y

1 Introduction

Human-robot collaboration has been expanding in recent years in a variety of fields ranging from industrial to domestic environments. The driving force behind the integration of such collaboration is the fact that the complementary capabilities of humans and robots can be merged: cognitive skills on the one hand and robustness and precision abilities on the other. Collaboration can be intended to different extents: *(i)* it can envisage pure workspace sharing in which human and robot work on autonomous or coordinated tasks without barriers between them or *(ii)* it can foresee voluntary exchange of forces between them to achieve a common objective.

In regard to the first scenario, the robot control strategy is generally supposed to guarantee the avoidance of any collision between the robot and the human in order to prevent human injury. As an example, possible approaches to the purpose are based on undertaking evasive actions to distance the robot from the person as in [1] or on dynamic trajectory scaling as in [2].

The approaches mentioned so far aim at assisting the human operator regardless of possible robot autonomous tasks, i.e. they build on a leader-follower architecture in which the human acts as leader and the robot only plays a follower role aimed at minimizing the leader effort. However, as reported in [3] and [4], increasing attention is being devoted to *shared control* scenarios in which, as it happens in the case of *human-human* interaction, the robot autonomy is preserved to a certain extent and equal roles are attributed to both robotic and human counterparts. The shared control paradigm arises in teleoperation scenarios [4] where the human operator typically provides control inputs via haptic interface, while the robotic system preserves autonomous behaviors, as instance, for collision avoidance [5]. More recently, this paradigm has also been successfully explored in contexts of physical human-robot interaction. A solution based on game theory is presented in [6] where human and robot are assumed to optimize the same cost function. In the proposed approach, the human and robot roles are continuously adapted on the basis of the human exerted force: the higher the force, the higher the influence of the human intended motion. The work in [7] proposes to achieve the same behavior by deforming the robot trajectory in dependence of the exerted human forces and formulates a constrained optimization problem to the purpose. A heuristic agreement index is designed in [8] so that, if the forces of robot and human agree, the robot acts as leader, otherwise as follower. Finally, a solution based on data-driven stochastic modeling is devised in [9] where a risk sensitive optimization problem is defined to tackle the uncertainty in the human behavior model.

In addition, it is worth noticing that, even in the context of human-robot collaboration, the use of *multiple* robots can significantly improve the overall system performance in terms of possible payload and robustness with respect to the single robot case. In this scenario, in addition to the aspects highlighted above, the problem of *coordinating* the multi-robot system, while achieving the desired interaction, arises as well. Moreover, as also encouraged by the

strategic initiative of Industry 4.0, a decentralized implementation of the multi-robot control algorithm also increases the flexibility and reconfigurability of the work-cell, which are desirable features in a human multi-robot collaboration strategy. More in detail, in this paper we consider a scenario of physical human multi-manipulator interaction where the human and the robots co-manipulate the same object. In this context, the following additional issues need to be addressed with respect to the case of single robot single human interaction:

- since the human does not directly interact with one of the robots but with the co-manipulated object, the human interaction wrench needs to be estimated for pursuing any interaction strategy. The problem is particularly challenging when no force sensors are adopted to measure the human wrench and in absence of a central control unit;
- internal wrenches are required to be regulated during cooperative manipulation in order not to damage the object and/or the manipulators. In this regard, the computation of internal wrenches is coupled with the one of the human-robot one;
- at low level, specific actions need to be included to synchronize the tracking errors, counteract model uncertainties and reduce internal wrenches in transient phase.

Despite its potentiality, few investigations are available in literature in regard to this scenario which, in particular, is only addressed [8] where heuristics are adopted to modulate the human collaboration and a centralized solution is presented.

Motivated by these reasons, we propose a distributed control framework for optimal human multi-robot shared control of a common object which is tightly grasped by manipulators and which the human physically interacts with. In particular, we propose a two layer architecture where the optimal object motion comes as the solution of a LQT problem which takes into account both robots and human intentions, being the latter estimated by resorting to RLS techniques and assuming a spring-damper model with unknown parameters for the human arm end point. The object motion is the input of the bottom layer which is in charge of coordinating the robots to track the desired motion. To this aim, an adaptive local control law is proposed which copes both with possible model uncertainties and internal stresses. The overall solution is first designed and presented in the framework of a centralized architecture and, then, a distributed version is provided by resorting to a leader-follower paradigm and to distributed observers. To the best of the authors' knowledge, this is the first work which combines LQT and human intention estimation in the way described in the following and proposes an enough general framework for *distributed* human multi-robot physical interaction. The approach can be applied to any cooperative manipulation task which involves the specification of an object trajectory. This includes, by resorting to the list of applications identified in the survey in [10], applications such as handling, assembly and welding in any of which the human operator may wish to intervene during the

robots' activity to correct the task or to participate in it and, to this end, the proposed shared control strategy can be applied.

Summarizing, the main contributions of the paper are the following:

- a novel shared control strategy in the framework of optimal control is presented. The role of the robots is dynamically adapted depending on the estimation of the human arm parameters and takes into account the uncertainty of the latter;
- the case of multi-manipulator systems is tackled for the first time. This case poses additionally issues with respect to the single manipulator case, due to the necessity to handle internal wrenches in addition to external one in order to no affect the human-object interaction dynamics. Moreover, a sensor-less solution is adopted in which both the interaction with the human and internal wrenches are estimated by resorting to a momentum based approach;
- the solution presented is completely decentralized since the local control strategy only relies on information locally available.

The paper builds on the work in [11], from which inherits part of the overall architecture but differs from it with regard to the following points: i) a pure assistance task is considered in [11] while a shared control scenario is hereby analyzed, ii) an extension of the low-level control law is provided in this paper along with a more formal proof, iii) the assumption that the human exerted force is known by each robot is removed and an observer system is designed to the purpose, iv) the estimation of the human model is introduced.

The remainder of the paper is organized as follows. In Section 2, robot, object, inter-robot communication and human arm end point modeling are presented. In the same section, the formal statement of problem addressed in this work is provided. A centralized solution to this problem is detailed in Section 3 and is then extended to a distributed setting in Section 4. Finally, simulation results are provided in Section 5, while conclusions and future works are drawn in Section 6.

2 Mathematical background

Let us consider a system composed of N serial-chain mobile manipulators which tightly grasp a rigid object and a human operator that co-manipulates the same object as in Figure 1. In the rest of the paper, when we refer to *human interaction*, we intend that the human operator exerts, through his/her hand, forces on the the object that is tightly co-manipulated by the multi-robot system. In this way, the human is able to modify the object motion according to his/her desired motion.

In the figure, the following reference frames are defined:

- Σ_w is the world reference frame;
- Σ_o is the object reference frame;
- $\Sigma_{r,i}$ is the reference frame attached to the end effector of the i th robot;

– Σ_h is the reference frame attached to the human arm end point.

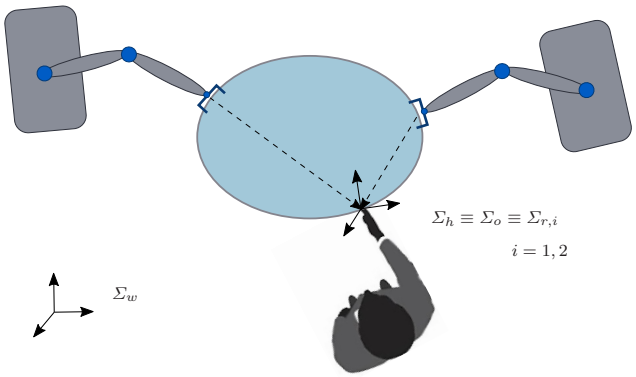

Fig. 1 Representation of the considered system composed of multiple robots physically interacting with a human operator; the reference frames Σ_w, Σ_h, Σ_o and $\Sigma_{r,i}$ are reported.

Without loss of generality, the following assumption is considered.

Assumption 1 *Robot kinematics and dynamics in the operational space are referred to the human arm end point frame Σ_h (i.e., $\Sigma_{r,i} \equiv \Sigma_h$, $\forall\, i$). At the same way, the object dynamics is referred to the same frame Σ_h (i.e., $\Sigma_o \equiv \Sigma_h$).*

The above assumption is not unrealistic in many practical scenarios since the geometry of the object is known or can be estimated beforehand.
For the sake of readability the time-dependence of the variables will be omitted in the following, if not strictly necessary. Moreover, we report in the Table 1 below a brief description of the notation used in the rest of the paper in terms of subscripts, superscripts and main variables adopted.

2.1 Robot modeling

The operational space dynamics of robot i away from kinematic singularities can be expressed as [12]

$$\begin{aligned} \boldsymbol{M}_i(\boldsymbol{x}_i)\ddot{\boldsymbol{x}}_i + \boldsymbol{C}_i(\boldsymbol{x}_i, \dot{\boldsymbol{x}}_i)\dot{\boldsymbol{x}}_i + \boldsymbol{\eta}_i(\boldsymbol{x}_i, \dot{\boldsymbol{x}}_i) &= \boldsymbol{u}_i - \boldsymbol{h}_i \\ &= \boldsymbol{Y}_i(\boldsymbol{x}_i, \dot{\boldsymbol{x}}_i, \ddot{\boldsymbol{x}}_i)\boldsymbol{\pi}_i \end{aligned} \tag{1}$$

where $\boldsymbol{u}_i \in \mathbb{R}^p$ is the control input, $\boldsymbol{x}_i = \left[\boldsymbol{p}_i^{\mathrm{T}} \ \boldsymbol{\phi}_i^{\mathrm{T}}\right]^{\mathrm{T}} \in \mathbb{R}^p$ is the end effector configuration in terms of position, $\boldsymbol{p}_i$, and orientation, $\boldsymbol{\phi}_i$, of frame $\Sigma_{r,i}$ with respect to Σ_w, $\boldsymbol{M}_i \in \mathbb{R}^{p \times p}$ is the symmetric positive definite inertia matrix,

Table 1 Table of symbols

Variable	Description
N	Number of robots
γ, Γ	Scalar variables are denoted by lowercase or uppercase letters and in italic
$\boldsymbol{\gamma}$	Vectors are denoted by lowercase letters and boldface
$\boldsymbol{\Gamma}$	Matrices are denoted by uppercase letters and boldface
$\boldsymbol{x}_i \in \mathbb{R}^p$	Configuration (position and orientation) of the i th robot end effector
$\boldsymbol{p}_h \in \mathbb{R}^m$	Position of the human arm end point
$\boldsymbol{x}_o \in \mathbb{R}^p$	Object configuration
$\boldsymbol{x}_v \in \mathbb{R}^p$	Desired configuration of the object to be tracked by the robot system
$\boldsymbol{h}_i \in \mathbb{R}^p$	Interaction wrench at the i th robot end effector
$\boldsymbol{h}_h \in \mathbb{R}^p$	Wrench exerted by the human operator on the object being manipulated
$\boldsymbol{h}_{int} \in \mathbb{R}^{Np}$	Internal wrench exerted by robots on the object
$\boldsymbol{h}_{int,i} \in \mathbb{R}^p$	Contribution of the i th robot to the internal wrench
$\boldsymbol{u}_i \in \mathbb{R}^p$	Input of the i th robot
$\boldsymbol{\pi}_i \in \mathbb{R}^{n_{\pi_i}}$	Dynamic parameters of the i th robot
$\hat{(\cdot)}$	Estimation of a *local* variable, e.g. $\hat{\boldsymbol{h}}_{int,i}$ is the estimation made by robot i of $\boldsymbol{h}_{int,i}$
${}^i\hat{(\cdot)}$	Estimation of a *global* variable made by robot i, e.g. ${}^i\hat{\boldsymbol{x}}_v$ is the estimation made by robot i of $\boldsymbol{x}_v$
$\boldsymbol{h}^d_{int,i}$	Desired value of $\boldsymbol{h}_{int,i}$
$\boldsymbol{e}_{int,i}$	Internal wrench tracking error of robot i $\boldsymbol{e}_{int,i} = \boldsymbol{h}^d_{int,i} - \boldsymbol{h}_{int,i}$
$\hat{\boldsymbol{e}}_{int,i}$	Estimation made by robot i of the internal wrench tracking error $\hat{\boldsymbol{e}}_{int,i} = \boldsymbol{h}^d_{int,i} - \hat{\boldsymbol{h}}_{int,i}$
$\tilde{\boldsymbol{h}}_{int,i}$	Estimation error made by robot i of its internal wrench $\tilde{\boldsymbol{h}}_{int,i} = \boldsymbol{h}_{int,i} - \hat{\boldsymbol{h}}_{int,i}$
${}^i\tilde{\boldsymbol{h}}_h$	Estimation error made by robot i of the human wrench ${}^i\tilde{\boldsymbol{h}}_h = \boldsymbol{h}_h - {}^i\hat{\boldsymbol{h}}_h$
$\boldsymbol{O}_{n\times m}$	Matrix with dimension $n \times m$ of all elements equal to 0
$\boldsymbol{I}_m$ $(\boldsymbol{O}_m)$	Square identity (null) matrix with dimension $m \times m$
$\boldsymbol{0}_m$	Column vector with m elements equal to 0

$\boldsymbol{C}_i \in \mathbb{R}^{p\times p}$ is the centrifugal and Coriolis terms matrix, $\boldsymbol{\eta}_i \in \mathbb{R}^p$ is the viscous friction and gravity terms vector and $\boldsymbol{h}_i = \begin{bmatrix} \boldsymbol{f}_i^{\mathrm{T}} & \boldsymbol{\tau}_i^{\mathrm{T}} \end{bmatrix}^{\mathrm{T}} \in \mathbb{R}^p$ is the vector of interaction wrenches between the end effector and the grasped object, composed of force, $\boldsymbol{f}_i$, and torque, $\boldsymbol{\tau}_i$, components. In addition, $\boldsymbol{Y}_i \in \mathbb{R}^{p\times n_{\pi_i}}$ is the regressor matrix and $\boldsymbol{\pi}_i \in \mathbb{R}^{n_{\pi_i}}$ is the constant vector of the dynamic parameters of the robot. By adopting Christoffel symbols of the first kind associated with the matrix $\boldsymbol{M}_i$ for $\boldsymbol{C}_i$, the following property holds true [13].

Property 1 Matrix $\dot{\boldsymbol{M}}_i - 2\boldsymbol{C}_i$ is skew-symmetric such that $\boldsymbol{v}^{\mathrm{T}}(\dot{\boldsymbol{M}}_i - 2\boldsymbol{C}_i)\boldsymbol{v} = 0$, $\forall\, \boldsymbol{v} \in \mathbb{R}^p$.

Note that in our framework robots can be heterogeneous and redundant. Finally, as typical of real settings, it is supposed that only an estimate of model (1) is available:

$$\hat{\boldsymbol{M}}_i\ddot{\boldsymbol{x}}_i + \hat{\boldsymbol{C}}_i\dot{\boldsymbol{x}}_i + \hat{\boldsymbol{\eta}}_i = \boldsymbol{Y}_i(\boldsymbol{x}_i, \dot{\boldsymbol{x}}_i, \ddot{\boldsymbol{x}}_i)\hat{\boldsymbol{\pi}}_i = \boldsymbol{u}_i - \boldsymbol{h}_i - \boldsymbol{Y}_i(\boldsymbol{x}_i, \dot{\boldsymbol{x}}_i, \ddot{\boldsymbol{x}}_i)\tilde{\boldsymbol{\pi}}_i \tag{2}$$

where $\tilde{\boldsymbol{\pi}}_i = \boldsymbol{\pi}_i - \hat{\boldsymbol{\pi}}_i$ and the symbol $\hat{\cdot}$ denotes the estimate of the corresponding quantity.
In what follows, we refer to the notation in Table 1 concerning the identity matrix and the zero matrix/vector.

2.2 Human arm end point modeling

The model assumed for the human arm end point, which will be referred to as human model in the following, is

$$-\boldsymbol{D}_h\dot{\boldsymbol{p}}_h + \boldsymbol{K}_h(\boldsymbol{p}_{h,d} - \boldsymbol{p}_h) = \boldsymbol{f}_h \tag{3}$$

where $\boldsymbol{f}_h \in \mathbb{R}^m$ is the vector of the forces exerted by the human, $\boldsymbol{p}_h \in \mathbb{R}^m$ is the human arm end point position, which will be referred to as human position, with respect to Σ_w, $\boldsymbol{p}_{h,d} \in \mathbb{R}^m$ is the human desired position and $\boldsymbol{D}_h \in \mathbb{R}^{m\times m}$ and $\boldsymbol{K}_h \in \mathbb{R}^{m\times m}$ are the matrices that regulate the human damping and stiffness actions, respectively. As stated, for example in [14] and [15], these matrices are generally time-varying and their variation depends on the activation of the human arm muscles. The model in (3) is commonly assumed as representative for the human arm end point, e.g. in [16–18], and its validation can be found, for instance, in [14,19] with the inertial term shown to be negligible compared to damping and stiffness. Moreover, by following the assumptions in [16,18,20], the decoupling of the impedance parameters in the different directions is assumed, i.e., $\boldsymbol{D}_h = \mathrm{diag}(\boldsymbol{d}_h)$ and $\boldsymbol{K}_h = \mathrm{diag}(\boldsymbol{k}_h)$ with $\boldsymbol{d}_h \in \mathbb{R}^m$ and $\boldsymbol{k}_h \in \mathbb{R}^m$. Then, the model in (3) can be rewritten as

$$\boldsymbol{Y}_h(\boldsymbol{p}_h, \dot{\boldsymbol{p}}_h)\boldsymbol{\pi}_h = \boldsymbol{f}_h \tag{4}$$

with

$$\begin{aligned} \boldsymbol{Y}_h &= [-\mathrm{diag}(\dot{\boldsymbol{p}}_h)\ -\mathrm{diag}(\boldsymbol{p}_h)\ \boldsymbol{I}_m] \in \mathbb{R}^{m\times 3m} \\ \boldsymbol{\pi}_h &= [\boldsymbol{d}_h^{\mathrm{T}}\ \boldsymbol{k}_h^{\mathrm{T}}\ \boldsymbol{p}_{h,d}^{\mathrm{T}}\boldsymbol{K}_h]^{\mathrm{T}} \in \mathbb{R}^{3m} \end{aligned} \tag{5}$$

It is worth remarking that the human parameters in $\boldsymbol{\pi}_h$ are *unknown* and might be time-varying.

2.3 Object modeling

Concerning the object dynamics, it holds

$$\boldsymbol{M}_o\ddot{\boldsymbol{x}}_o + \boldsymbol{C}_o(\boldsymbol{x}_o, \dot{\boldsymbol{x}}_o)\dot{\boldsymbol{x}}_o + \boldsymbol{g}_o = \sum\nolimits_{i=1}^{N} \boldsymbol{G}_i\boldsymbol{h}_i + \boldsymbol{h}_h \tag{6}$$

where $\boldsymbol{x}_o = \begin{bmatrix}\boldsymbol{p}_o^{\mathrm{T}} & \boldsymbol{\phi}_o^{\mathrm{T}}\end{bmatrix}^{\mathrm{T}} \in \mathbb{R}^p$ represents the configuration in terms of position $\boldsymbol{p}_o$ and orientation $\boldsymbol{\phi}_o$ of the object reference frame Σ_o with respect to Σ_w, $\boldsymbol{M}_o \in \mathbb{R}^{p\times p}$ is the inertia matrix, $\boldsymbol{C} \in \mathbb{R}^{p\times p}$ is the matrix of centrifugal and Coriolis terms, $\boldsymbol{g}_o \in \mathbb{R}^p$ is the vector of the gravity terms, $\boldsymbol{G}_i \in \mathbb{R}^{p\times p}$ is the grasping matrix associated with the ith robot for which, in light of Assumption 1, it holds $\boldsymbol{G}_i = \boldsymbol{I}_p\, \forall i$ and $\boldsymbol{h}_h = \boldsymbol{G}_h\boldsymbol{f}_h \in \mathbb{R}^p$ is the human wrench with $\boldsymbol{G}_h = [\boldsymbol{I}_m\ \boldsymbol{O}_m]^{\mathrm{T}} \in \mathbb{R}^{p\times m}$.
By denoting with $\boldsymbol{h}$ the stacked vector of the interaction wrenches and with $\boldsymbol{G}$ the collective grasping matrix, i.e.

$$\boldsymbol{h} = [\boldsymbol{h}_1^{\mathrm{T}}\ \dots\ \boldsymbol{h}_N^{\mathrm{T}}]^{\mathrm{T}} \in \mathbb{R}^{Np},\ \boldsymbol{G} = [\boldsymbol{G}_1\ \dots\ \boldsymbol{G}_N] \in \mathbb{R}^{p\times Np}$$

the interaction wrenches can be divided into external $\boldsymbol{h}_e \in \mathbb{R}^{Np}$ and internal $\boldsymbol{h}_{int} \in \mathbb{R}^{Np}$ components [21], i.e., those that contribute and do not contribute, respectively, to the object motion for which it holds

$$\boldsymbol{h} = \boldsymbol{h}_e + \boldsymbol{h}_{int} = \boldsymbol{G}^{\dagger}\boldsymbol{G}\boldsymbol{h} + (\boldsymbol{I}_{Np} - \boldsymbol{G}^{\dagger}\boldsymbol{G})\boldsymbol{h} \tag{7}$$

Finally, the following assumption is considered.

Assumption 2 *The kinematic and dynamic parameters of the manipulated object model are known.*

This hypothesis can be easily overcome by resorting to *ad-hoc* techniques that allow to distributively estimate these parameters by properly interacting with the object like in [22].

2.4 Communication modeling

Since we aim at devising a distributed framework, a brief review of graph theory is provided. The information exchange between the robots is modeled by a connectivity graph $\mathcal{G}(\mathcal{E}, \mathcal{V})$ where $\mathcal{V}$ is the set of vertices representing the robots, and $\mathcal{E} = \mathcal{V} \times \mathcal{V}$ is the set of edges representing the communication links, that is the ith robot can send information to the jth robot if the condition $(i,\, j) \in \mathcal{E}$ holds. The set of neighbors of the ith robot from which it receives information is defined as $\mathcal{N}_i = \{j \in \mathcal{V} :\ (j, i) \in \mathcal{E}\}$. The topology of the graph is described in terms of the $(N \times N)$ Laplacian matrix $\boldsymbol{L} = \{l_{ij}\}$ such that $l_{ii} = \sum_{j=1, j\neq i}^{N} a_{ij}$ and $l_{ij} = -a_{ij}$ when $i \neq j$, being $a_{ij} = 1$ if the jth robot can send information to ith robot (i.e. $(j, i) \in \mathcal{E}$), and 0 otherwise. Moreover, by construction, zero is always a right eigenvalue of the Laplacian matrix with

the corresponding right eigenvector ($N \times 1$) vector of all ones [23]. Therefore, $\text{rank}(\boldsymbol{L}) \leq N-1$ where the equality holds when the graph is connected. In this paper, we assume the communication graph is undirected and connected, i.e. all the edges are bi-directional and any couple of vertices of the graph can always be connected by an undirected path. Moreover, the approach requires information to be explicitly exchanged between robots; however, this is not an issue in practical scenarios since all mobile manipulators have such communication capabilities.

2.5 Problem formulation

We can now state the main problem addressed in this work.

Problem 1 Let us consider a multi-robot system composed of N manipulators rigidly grasping an object which a human operator is interacting with. Let us assume that a central unit is not available and that a robots' desired trajectory $\boldsymbol{x}_{r,d} \in \mathbb{R}^p$ (with derivative $\dot{\boldsymbol{x}}_{r,d} \in \mathbb{R}^p$) is assigned to the object as well as a desired internal wrench $\boldsymbol{h}_{int}^d \in \mathbb{R}^{Np}$ is given. The objective is to design the robot control input $\boldsymbol{u}_i$ ($i = 1, 2, \ldots, N$) in (1) such that the manipulated object behaves according to the following dynamics

$$\boldsymbol{M}_v \ddot{\boldsymbol{x}}_v = \boldsymbol{u}_v \tag{8}$$

where $\boldsymbol{M}_v \in \mathbb{R}^{p \times p}$ is the virtual inertia matrix, $\boldsymbol{x}_v = \begin{bmatrix} \boldsymbol{p}_v^{\mathrm{T}} & \boldsymbol{\phi}_v^{\mathrm{T}} \end{bmatrix}^{\mathrm{T}} \in \mathbb{R}^p$ is the configuration of the virtual object and $\boldsymbol{u}_v \in \mathbb{R}^p$ represents the virtual input to be defined so as to optimize the following cost function

$$\begin{aligned} J = \frac{1}{2} \int_{t_0}^{+\infty} \Big(& \underbrace{(\bar{\boldsymbol{x}}_v - \bar{\boldsymbol{x}}_{r,d})^{\mathrm{T}} \boldsymbol{Q}_{r,d} (\bar{\boldsymbol{x}}_v - \bar{\boldsymbol{x}}_{r,d})}_{i} + \underbrace{\boldsymbol{u}_v^{\mathrm{T}} \boldsymbol{R}_v \boldsymbol{u}_v}_{ii} \\ & + \underbrace{(\bar{\boldsymbol{x}}_v - \bar{\boldsymbol{x}}_{h,d})^{\mathrm{T}} \boldsymbol{Q}_{h,d} (\bar{\boldsymbol{x}}_v - \bar{\boldsymbol{x}}_{h,d})}_{iii} + \underbrace{\boldsymbol{f}_h^{\mathrm{T}} \boldsymbol{R}_h \boldsymbol{f}_h}_{iv} \Big) dt \end{aligned} \tag{9}$$

where $\bar{\boldsymbol{x}}_v = \begin{bmatrix} \boldsymbol{x}_v^{\mathrm{T}} & \dot{\boldsymbol{x}}_v^{\mathrm{T}} \end{bmatrix}^{\mathrm{T}} \in \mathbb{R}^{2p}$ is the aggregate vector of state, $\bar{\boldsymbol{x}}_{r,d} = \begin{bmatrix} \boldsymbol{x}_{r,d}^{\mathrm{T}} & \dot{\boldsymbol{x}}_{r,d}^{\mathrm{T}} \end{bmatrix}^{\mathrm{T}} \in \mathbb{R}^{2p}$ and $\bar{\boldsymbol{x}}_{h,d} = \begin{bmatrix} \boldsymbol{p}_{h,d}^{\mathrm{T}} & \boldsymbol{0}_{2p-m}^{\mathrm{T}} \end{bmatrix}^{\mathrm{T}} \in \mathbb{R}^{2p}$ are the aggregate vectors of the robots and human desired trajectory, respectively, $\boldsymbol{R}_h \in \mathbb{R}^{m \times m}$ and $\boldsymbol{R}_v \in \mathbb{R}^{p \times p}$ are symmetric positive definite matrices, $\boldsymbol{Q}_{r,d} \in \mathbb{R}^{2p \times 2p}$ is a symmetric positive semi-definite matrix, $\boldsymbol{Q}_{h,d} \in \mathbb{R}^{2p \times 2p}$ is defined as

$$\boldsymbol{Q}_{h,d} = \boldsymbol{S}^{\mathrm{T}} \boldsymbol{W}_{h,d} \boldsymbol{S}, \quad \boldsymbol{S} = \begin{bmatrix} \boldsymbol{I}_m & \boldsymbol{O}_{m \times 2p-m} \\ \boldsymbol{O}_{m \times 2p-m} & \boldsymbol{I}_m \end{bmatrix} \tag{10}$$

being $\boldsymbol{W}_{h,d} \in \mathbb{R}^{2m \times 2m}$ a symmetric positive semi-definite weighting matrix. In addition, internal wrench regulation is required, i.e. $\boldsymbol{h}_{int} \to \boldsymbol{h}_{int}^d$.

The rationale behind (9) is to continuously combine the robots desired trajectory for the object (i) with the human desired one (iii) and, similarly, to x the effort of the robots (ii) and of the human (iv) on the basis of the respective weighting matrices. This means that by increasing $\boldsymbol{Q}_{h,d}$ and $\boldsymbol{R}_h$ with respect to $\boldsymbol{Q}_{r,d}$ the human intention overtakes the robots one (and vice-versa) according to an optimal formulation. In addition, the proposed approach is also suitable for an assistance task, whose aim is to minimize the human effort, by setting $\boldsymbol{Q}_{r,d} = \boldsymbol{O}_{2p}$.

In the above formulation the human intention in terms of object orientation is not taken into account which means that robots have full control on it. Like in [24], this is motivated by the fact that the human is in charge of modifying the object motion while robots autonomously and precisely control the orientation.

In what follows, first a centralized solution to the Problem 1 is provided in Section 3; then, building on this, a distributed solution to the same problem is presented in Section 4.

3 Centralized solution

A two layer architecture depicted in Figure 2 is devised. The high-level is in charge of defining the object reference trajectory $\boldsymbol{x}_v$ as solution of the optimal problem in (9) on the basis of human intentions and the low-level of defining the local control inputs $\boldsymbol{u}_i$ in (1) to actually track the trajectory while achieving wrench regulation.

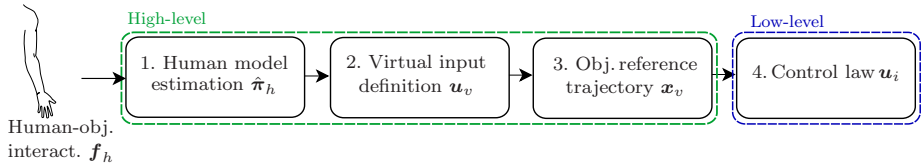

Fig. 2 Two-layer architecture of the proposed solution.

Concerning the high-level, the formulation in (8) requires the virtual input $\boldsymbol{u}_v$ to be designed (block 2) so as to optimize (9). By replacing the human model (3) in the cost function (9), the latter can be rewritten as

$$J = \frac{1}{2}\int_{t_0}^{+\infty} \Big((\bar{\boldsymbol{x}}_v - \bar{\boldsymbol{x}}_{r,d})^{\mathrm{T}} \boldsymbol{Q}_{r,d} (\bar{\boldsymbol{x}}_v - \bar{\boldsymbol{x}}_{r,d}) + \boldsymbol{u}_v^{\mathrm{T}} \boldsymbol{R}_v \boldsymbol{u}_v + (\bar{\boldsymbol{x}}_v - \bar{\boldsymbol{x}}_{h,d})^{\mathrm{T}} \bar{\boldsymbol{Q}}_h (\bar{\boldsymbol{x}}_v - \bar{\boldsymbol{x}}_{h,d}) \Big) dt \tag{11}$$

with $\bar{\boldsymbol{Q}}_h = \boldsymbol{S}^{\mathrm{T}} \bar{\boldsymbol{W}}_{h,d} \boldsymbol{S}$ and

$$\bar{\boldsymbol{W}}_{h,d} = \boldsymbol{W}_{h,d} + \begin{bmatrix} \boldsymbol{K}_h^{\mathrm{T}} \boldsymbol{R}_h \boldsymbol{K}_h & \boldsymbol{K}_h^{\mathrm{T}} \boldsymbol{R}_h \boldsymbol{D}_h \\ \boldsymbol{D}_h^{\mathrm{T}} \boldsymbol{R}_h \boldsymbol{K}_h & \boldsymbol{D}_h^{\mathrm{T}} \boldsymbol{R}_h \boldsymbol{D}_h \end{bmatrix} \tag{12}$$

It is worth noticing that, according to (12), the weight associated with the human desired motion dynamically adapts on the basis of the human impedance parameters $\boldsymbol{K}_h$ and $\boldsymbol{D}_h$, e.g., when the human stiffens the arm (i.e., $\boldsymbol{K}_h$ increases) the corresponding quantities in $\bar{\boldsymbol{Q}}_h$ *automatically* increase as well.
The formulation in (11)-(12) shows the dependence of the objective function on the *unknown* human parameters $\boldsymbol{K}_h, \boldsymbol{D}_h, \boldsymbol{p}_{h,d}$, that is on $\boldsymbol{\pi}_h$ in (5). Therefore, an online estimation of these parameters is needed by exploiting the knowledge of human force and motion, i.e. $\boldsymbol{f}_h$, $\boldsymbol{p}_h$, $\dot{\boldsymbol{p}}_h$ (block 1 in Figure 2), and is then used to find $\boldsymbol{u}_v$ which minimizes (11). Afterwards, the virtual object trajectory $\boldsymbol{x}_v$ is computed according to the dynamics in (8) (block 3) and is adopted by the robots as actual reference trajectory for the object. In particular, a standard control law for trajectory tracking with internal force regulation as in [25] can be leveraged at this point for the low-level *centralized* solution (block 4) and details are here omitted since a distributed solution to this problem is presented in next sections.

3.1 Human parameters estimation

A Recursive Least Square method with forgetting factor is here proposed to estimate the human arm parameter $\boldsymbol{\pi}_h$. Let us consider that the measurements are acquired at each kT, with $k \in \mathbb{N}$ the discrete time index and $T \in \mathbb{R}$ the sampling time, and let us denote with $(\cdot)_k$ the corresponding quantity at time kT. The estimation error $\boldsymbol{e}_{h,k} \in \mathbb{R}^m$ is defined as

$$\boldsymbol{e}_{h,k} = \boldsymbol{f}_{h,k} - \boldsymbol{Y}_{h,k}\hat{\boldsymbol{\pi}}_{h,k-1} \tag{13}$$

where $\boldsymbol{Y}_{h,k}$ is the human regressor defined in (4) and $\hat{\boldsymbol{\pi}}_{h,k} \in \mathbb{R}^{3m}$ is the estimate of the unknown human parameters.

Remark 1 The computation of (13) requires the knowledge of $\boldsymbol{f}_h$ which, in the centralized case, can be retrieved from the collective wrench $\boldsymbol{h}$ and the knowledge of the object dynamics in (6) as in [26].

By leveraging [27], the parameters estimate is updated as

$$\hat{\boldsymbol{\pi}}_{h,k} = \hat{\boldsymbol{\pi}}_{h,k-1} + \boldsymbol{L}_k \boldsymbol{e}_{h,k} \tag{14}$$

where the matrices $\boldsymbol{L}_k \in \mathbb{R}^{3m \times m}$ and $\boldsymbol{P}_k \in \mathbb{R}^{3m \times 3m}$ are

$$\begin{aligned} \boldsymbol{L}_k &= \boldsymbol{P}_{k-1}\boldsymbol{Y}_{h,k}^{\mathrm{T}}(\lambda \boldsymbol{I}_m + \boldsymbol{Y}_{h,k}\boldsymbol{P}_{k-1}\boldsymbol{Y}_{h,k}^{\mathrm{T}})^{-1} \\ \boldsymbol{P}_k &= \frac{1}{\lambda}(\boldsymbol{I}_{3m} - \boldsymbol{L}_k\boldsymbol{Y}_{h,k})\boldsymbol{P}_{k-1} \end{aligned} \tag{15}$$

being $\lambda \in (0,\, 1]$ the forgetting factor which regulates the amount of data to be forgotten at each estimate update: the lower the forgetting factor, the lower the weight associated with past inputs. This implies that the lower the forgetting factor, the more the estimation is able to track changes in the parameters but the more the misadjustment and the possible instability [27]. Implementation

details of (14) and (15) are not addressed here but a detailed discussion can be found in [28].
However, in order for the estimate $\hat{\boldsymbol{\pi}}_h$ in (14) to converge to the real values $\boldsymbol{\pi}_h$, the estimator input variables, i.e. $\boldsymbol{p}_h$ and $\dot{\boldsymbol{p}}_h$, have to satisfy the persistence of excitation condition for which the approximation proposed in [29] is here considered, that is the following condition should be verified

$$\|\boldsymbol{P}_{k-1}\boldsymbol{Y}_{h,k}\| > \alpha, \quad \forall k \text{ with } \alpha \in \mathbb{R}^+ \tag{16}$$

Moreover, by leveraging the results in [18], a finite-time interval with predetermined duration Δ, during which the input signals are excited, allows the parameters to be estimated with a certain tolerance. For further details, the reader is referred to [18] and [29].
Based on the above considerations, we devise a confidence index $\mathcal{I}_c$ to establish the reliability of the human parameters estimate. The basic idea is that the latter is assumed reliable if there exists a time interval for which the system is "sufficiently" excited and as long as the estimation error is below a certain threshold, which leads to the following index

$$\mathcal{I}_c(\hat{\boldsymbol{\pi}}_{h,k}) = \begin{cases} 1, \text{if } \|\boldsymbol{e}_{h,k}\| < \bar{e} \wedge \exists\, k_1, k_2 \in \mathbb{N} : T|k_2 - k_1| \geq \Delta \\ \qquad\qquad \wedge\ \forall\, k \in [k_1,\, k_2] \text{ eq. (16) holds} \\ 0, \text{otherwise} \end{cases} \tag{17}$$

with $\bar{e} \in \mathbb{R}$ a positive constant representing the maximum allowed estimation error.
Finally, it is worth remarking that the focus of this work is not to provide a contribution to human parameter estimation. Hence, any other technique than RLS, as the approach in [30], might be used in block 1 of Figure 2.

3.2 Solution of the optimal LQT problem and virtual input $\boldsymbol{u}_v$ definition

The confidence index $\mathcal{I}_c$ specifies whether the human parameter estimation is reliable or not (as in the initial transient phase). Therefore, the latter case needs to be explicitly handled in order to avoid undesired interaction behavior. In detail, when $\mathcal{I}_c(\hat{\boldsymbol{\pi}}_{h,k}) = 0$, the estimate $\hat{\boldsymbol{\pi}}_{h,k}$ is discarded and full control of the system is given to the human operator (instead of minimizing (11)) by setting $\boldsymbol{u}_v$ in (8) as

$$\boldsymbol{u}_v = -\boldsymbol{D}_v\dot{\boldsymbol{x}}_v + \boldsymbol{\gamma}(\boldsymbol{h}_h)$$

which leads to the following virtual model

$$\boldsymbol{M}_v\ddot{\boldsymbol{x}}_v + \boldsymbol{D}_v\dot{\boldsymbol{x}}_v = \boldsymbol{\gamma}(\boldsymbol{h}_h) \tag{18}$$

where $\boldsymbol{D}_v \in \mathbb{R}^{p\times p}$ represents a damping matrix and $\boldsymbol{\gamma}(\cdot) : \mathbb{R}^p \to \mathbb{R}^p$ is a function of the human wrench possibly chosen as a deadzone function with

threshold $t_h \in \mathbb{R}^+$, that is

$$\boldsymbol{\gamma}(\boldsymbol{h}_h) = \begin{cases} \boldsymbol{K}_\gamma\big(\boldsymbol{h}_h - t_h \dfrac{\boldsymbol{h}_h}{\|\boldsymbol{h}_h\|}\big) & \text{if } \|\boldsymbol{h}_h\| > t_h \\ \boldsymbol{0}_p & \text{if } \|\boldsymbol{h}_h\| \leq t_h \end{cases} \tag{19}$$

with $\boldsymbol{K}_\gamma \in \mathbb{R}^{p\times p}$ a positive definite matrix. Dynamics in (18) allows the human to move the object with the robots executing no autonomous tasks. On the contrary, when $\mathcal{I}_c(\hat{\boldsymbol{\pi}}_{h,k}) = 1$, the human estimate is exploited to minimize the cost in (11). To this aim, the following lemma holds true.

Lemma 1 *Let us consider a time-invariant linear system*

$$\dot{\boldsymbol{x}} = \boldsymbol{A}\boldsymbol{x} + \boldsymbol{B}\boldsymbol{u} \tag{20}$$

with $\boldsymbol{x} \in \mathbb{R}^n$ and $\boldsymbol{u} \in \mathbb{R}^m$ the state and the input of the system, and $\boldsymbol{A} \in \mathbb{R}^{n\times n}$ and $\boldsymbol{B} \in \mathbb{R}^{n\times m}$ the dynamic and input matrices, respectively. Let us consider the following infinite-horizon cost function

$$J = \frac{1}{2}\int_{t_0}^{\infty}\Big((\boldsymbol{x}-\boldsymbol{r}_1)^{\mathrm{T}}\boldsymbol{Q}_1(\boldsymbol{x}-\boldsymbol{r}_1)+(\boldsymbol{x}-\boldsymbol{r}_2)^{\mathrm{T}}\boldsymbol{Q}_2(\boldsymbol{x}-\boldsymbol{r}_2)+\boldsymbol{u}^{\mathrm{T}}\boldsymbol{R}\boldsymbol{u}\Big)dt \tag{21}$$

with $\boldsymbol{r}_1 \in \mathbb{R}^n$ and $\boldsymbol{r}_2 \in \mathbb{R}^n$ reference signals, $\boldsymbol{Q}_1 \in \mathbb{R}^{n\times n}$ and $\boldsymbol{Q}_2 \in \mathbb{R}^{n\times n}$ symmetric semi-definite positive matrices and $\boldsymbol{R} \in \mathbb{R}^{m\times m}$ a symmetric definite positive matrix. If the pair $(\boldsymbol{A}, \boldsymbol{B})$ is reachable and the pair $(\boldsymbol{A}, [\boldsymbol{Q}_1\ \boldsymbol{Q}_2]^{\mathrm{T}})$ is observable, then the optimal control input minimizing (21) *is*

$$\boldsymbol{u} = -\boldsymbol{K}\boldsymbol{x} + \boldsymbol{R}^{-1}\boldsymbol{B}^{\mathrm{T}}\boldsymbol{v} \tag{22}$$

where $\boldsymbol{K} \in \mathbb{R}^{m\times n}$ is a gain matrix defined as

$$\begin{aligned} &\boldsymbol{K} = \boldsymbol{R}^{-1}\boldsymbol{B}^{\mathrm{T}}\boldsymbol{T} \\ &\boldsymbol{T}\boldsymbol{A}+\boldsymbol{A}^{\mathrm{T}}\boldsymbol{T}-\boldsymbol{T}\boldsymbol{B}\boldsymbol{R}^{-1}\boldsymbol{B}^{\mathrm{T}}\boldsymbol{T}+\boldsymbol{Q}_1+\boldsymbol{Q}_2=\boldsymbol{O}_n \end{aligned} \tag{23}$$

and $\boldsymbol{v} \in \mathbb{R}^n$ is an auxiliary signal that evolves according to

$$-\dot{\boldsymbol{v}} = (\boldsymbol{A}-\boldsymbol{B}\boldsymbol{K})^{\mathrm{T}}\boldsymbol{v} + \boldsymbol{Q}_1\boldsymbol{r}_1 + \boldsymbol{Q}_2\boldsymbol{r}_2 \tag{24}$$

Proof The result follows by considering an aggregate weighting matrix $\bar{\boldsymbol{Q}} = [\boldsymbol{Q}_1\ \boldsymbol{Q}_2]^{\mathrm{T}} \in \mathbb{R}^{2n\times n}$ with the aggregate reference signal $\bar{\boldsymbol{r}} = [\boldsymbol{r}_1^{\mathrm{T}}\ \boldsymbol{r}_2^{\mathrm{T}}]^{\mathrm{T}} \in \mathbb{R}^{2n}$ and by extending the reasoning presented in [31] for the LQT problem.

By recalling (8), the state vector $\bar{\boldsymbol{x}}_v$ evolves according to

$$\dot{\bar{\boldsymbol{x}}}_v = \begin{bmatrix} \boldsymbol{O}_p & \boldsymbol{I}_p \\ \boldsymbol{O}_p & \boldsymbol{O}_p \end{bmatrix}\bar{\boldsymbol{x}}_v + \begin{bmatrix} \boldsymbol{O}_p \\ \boldsymbol{M}_v^{-1} \end{bmatrix}\boldsymbol{u}_v \tag{25}$$

By noticing that (11) and (25) are in the form of (21) and (20), respectively, and that reachability and observability conditions are fulfilled, Lemma 1 applies. The optimal virtual input $\boldsymbol{u}_v$ for (11) can be thus defined according to (22), by considering the estimated human parameters $\hat{\boldsymbol{\pi}}_h$ in place of the respective values in the cost function (11).

4 Distributed solution

Based on the centralized solution in Section 3, the *distributed* control framework to solve Problem 1 is now presented. The basic idea is to provide a decentralized implementation of the centralized architecture in Figure 2 by estimating the needed *global* information, and without changing the human-object interaction behaviour regulated by (11). As shown in the following, since each robot has only access to the local wrench $\boldsymbol{h}_i$ and the human operator interacts with the object co-manipulated by *all* the robots, the main global quantities to be estimated are (i) the measure of the force $\boldsymbol{f}_h$ exerted by the human operator and (ii) the contribution of each robot to the internal wrenches $\boldsymbol{h}_{int}$ in (7). Moreover, concerning the human-robot interaction strategy, we propose a leader-follower approach in which the leader, based on the estimation of $\boldsymbol{f}_h$, executes the high-level strategy of the architecture in Figure 2 and computes the optimal object reference trajectory $\boldsymbol{x}_v$, $\dot{\boldsymbol{x}}_v$, as in the centralized counterpart, while the followers estimate this trajectory via decentralized observers. These quantities feed a low-level adaptive control law which allows each robot to track the reference trajectory while regulating the internal wrenches. The resulting architecture is shown in Figure 3 and details are in the following.

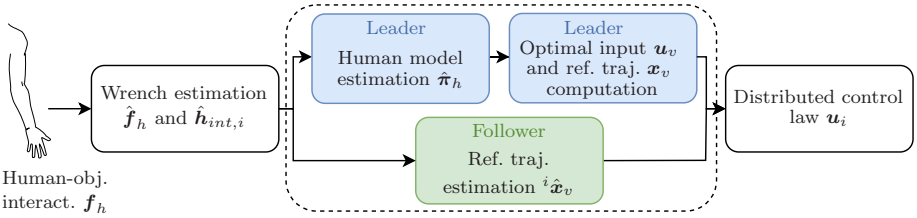

Fig. 3 Distributed architecture implemented by robot i. The dashed box denotes that, depending on the role of the robot, different blocks are executed: blue blocks on the top in the case of leader, green blocks on the bottom in the case of follower.

4.1 Distributed human and internal wrench estimation

Let us denote with $\boldsymbol{h}_{int,i}$ the ith sub-vector of $\boldsymbol{h}_{int}$ (i.e., the contribution of the ith robot to the internal wrenches $\boldsymbol{h}_{int}$). The objective is to define a local observer in order for the ith robot to estimate $\boldsymbol{h}_{int,i}$ as well as the human force $\boldsymbol{f}_h$ (or equivalently $\boldsymbol{h}_h$). In view of (7) and by introducing the following selection matrix $\boldsymbol{\Gamma}_i$

$$\boldsymbol{\Gamma}_i = \begin{bmatrix} \boldsymbol{O}_p & \dots & \underbrace{\boldsymbol{I}_p}_{robot\ i} & \dots & \boldsymbol{O}_p \end{bmatrix} \in \mathbb{R}^{p \times Np}$$

the vector $\boldsymbol{h}_{int,i}$ can be computed as

$$\begin{aligned}\boldsymbol{h}_{int,i} &= \boldsymbol{\Gamma}_i\boldsymbol{h}_{int} = \boldsymbol{h}_i - \boldsymbol{\Gamma}_i\boldsymbol{G}^\dagger\boldsymbol{G}\boldsymbol{h} = \boldsymbol{h}_i - \boldsymbol{\Gamma}_i\boldsymbol{G}^\dagger(\boldsymbol{G}_i\boldsymbol{h}_i + \sum_{j\neq i}\boldsymbol{G}_j\boldsymbol{h}_j) \\ &= \underbrace{(\boldsymbol{I}_p - \boldsymbol{\Gamma}_i\boldsymbol{G}^\dagger\boldsymbol{G}_i)\boldsymbol{h}_i}_{known} \underbrace{- \boldsymbol{\Gamma}_i\boldsymbol{G}^\dagger\sum_{j=1,j\neq i}^{N}\boldsymbol{G}_j\boldsymbol{h}_j}_{unknown} \end{aligned} \tag{26}$$

which is composed of a first local known term and a second unknown term depending on the wrenches exerted by the other robots. Thus, by considering the ith robot, the object model in (6) can be reformulated as

$$\boldsymbol{M}_o\ddot{\boldsymbol{x}}_o = \boldsymbol{G}_i\boldsymbol{h}_i + \sum_{j=1,j\neq i}^{N}\boldsymbol{G}_j\boldsymbol{h}_j + \boldsymbol{h}_h - \boldsymbol{C}_o\dot{\boldsymbol{x}}_o - \boldsymbol{g}_o \tag{27}$$

Based on the approach in [26], the following residual vector $\boldsymbol{\theta}_i(t) \in \mathbb{R}^p$ is introduced

$$\boldsymbol{\theta}_i(t) = \boldsymbol{K}_\theta\int_{t_0}^{t}(\boldsymbol{\alpha} - \boldsymbol{G}_i\boldsymbol{h}_i - \boldsymbol{\theta}_i)d\tau + \boldsymbol{K}_\theta\boldsymbol{m}(t) \tag{28}$$

with $\boldsymbol{K}_\theta \in \mathbb{R}^{p\times p}$ a constant diagonal positive definite matrix, $\boldsymbol{m}(t) = \boldsymbol{M}_o\dot{\boldsymbol{x}}_o$ the generalized momentum of the object and $\boldsymbol{\alpha} = \boldsymbol{g}_o - \frac{1}{2}\dot{\boldsymbol{x}}_o^{\mathrm{T}}\frac{\partial\boldsymbol{M}_o}{\partial\boldsymbol{x}_o}\dot{\boldsymbol{x}}_o$. From [26], it follows

$$\dot{\boldsymbol{\theta}}_i(t) = -\boldsymbol{K}_\theta\boldsymbol{\theta}_i(t) + \boldsymbol{K}_\theta\Big(\sum_{j=1,j\neq i}^{N}\boldsymbol{G}_j\boldsymbol{h}_j + \boldsymbol{h}_h\Big) \tag{29}$$

which represents a low-pass filter whose bandwidth depends on the gain matrix $\boldsymbol{K}_\theta \in \mathbb{R}^{p\times p}$ and which leads to

$$\boldsymbol{\theta}_i(t) \approx \sum_{j=1,j\neq i}^{N}\boldsymbol{G}_j\boldsymbol{h}_j(t) + \boldsymbol{h}_h(t), \quad \forall t \tag{30}$$

Thus, by replacing (30) in (26), it holds

$$\boldsymbol{h}_{int,i} = \boldsymbol{\Gamma}_i(\boldsymbol{I}_{Np} - \boldsymbol{G}^\dagger\boldsymbol{G})\boldsymbol{h} \approx (\boldsymbol{I}_p - \boldsymbol{\Gamma}_i\boldsymbol{G}^\dagger\boldsymbol{G}_i)\boldsymbol{h}_i - \boldsymbol{\Gamma}_i\boldsymbol{G}^\dagger(\boldsymbol{\theta}_i - \boldsymbol{h}_h) \tag{31}$$

Remark 2 By virtue of (30), the approximation error made in (31) about the computation of $\boldsymbol{h}_{int,i}$ is

$$\boldsymbol{h}_{int,i} - \Big((\boldsymbol{I}_p - \boldsymbol{\Gamma}_i\boldsymbol{G}^\dagger\boldsymbol{G}_i)\boldsymbol{h}_i - \boldsymbol{\Gamma}_i\boldsymbol{G}^\dagger(\boldsymbol{\theta}_i - \boldsymbol{h}_h)\Big) = \boldsymbol{\Gamma}_i\boldsymbol{G}^\dagger(\boldsymbol{\theta}_i - \sum_{j\neq i}\boldsymbol{G}_j\boldsymbol{h}_j - \boldsymbol{h}_h) \tag{32}$$

that is negligible only when the filter input (namely, $\sum_{j\neq i}\boldsymbol{G}_j\boldsymbol{h}_j + \boldsymbol{h}_h$) has a bandwidth much smaller than the cut-off frequency of the filter. Therefore, as made in [26] and citing works, a practical choice is to set $\boldsymbol{K}_\theta$ as high as possible subject to the potential digital implementation of the filter itself.

Equation (31) makes evident that $\boldsymbol{h}_{int,i}$ can not be computed without the knowledge of $\boldsymbol{h}_h$ which is unknown as well. In this regard, let us define the following auxiliary signal $\boldsymbol{\xi}_i \in \mathbb{R}^p$

$$\boldsymbol{\xi}_i = (\boldsymbol{I}_p - \boldsymbol{\Gamma}_i \boldsymbol{G}^\dagger \boldsymbol{G}_i)\boldsymbol{h}_i - \boldsymbol{\Gamma}_i \boldsymbol{G}^\dagger \boldsymbol{\theta}_i \tag{33}$$

which, in light of (31) and by computing the term $\boldsymbol{\Gamma}_i \boldsymbol{G}^\dagger$, can be rewritten as

$$\boldsymbol{\xi}_i \approx \boldsymbol{h}_{int,i} - \boldsymbol{\Gamma}_i \boldsymbol{G}^\dagger \boldsymbol{h}_h = \boldsymbol{h}_{int,i} - \frac{1}{N}\boldsymbol{h}_h \tag{34}$$

Note that neither $\boldsymbol{h}_{int,i}$ nor $\boldsymbol{h}_h$ are known in (34), but an approximation of $\boldsymbol{h}_{int,i} - \frac{1}{N}\boldsymbol{h}_h$ is provided by the right-hand side of (33), i.e. by the auxiliary variable $\boldsymbol{\xi}_i$. By resorting to the following lemma, the i th robot can compute the estimate ${}^i\hat{\boldsymbol{h}}_h \in \mathbb{R}^p$ of the human wrench $\boldsymbol{h}_h$ as well as the estimate $\hat{\boldsymbol{h}}_{int,i}$ of its contribution to the internal wrench.

Lemma 2 *Let each robot run the following observer*

$$\begin{cases} \dot{\boldsymbol{z}}_i = \gamma \sum\limits_{j \in \mathcal{N}_i} \text{sign}({}^j\hat{\boldsymbol{h}}_h - {}^i\hat{\boldsymbol{h}}_h) \\ {}^i\hat{\boldsymbol{h}}_h = \boldsymbol{z}_i - N\boldsymbol{\xi}_i \\ \hat{\boldsymbol{h}}_{int,i} = \boldsymbol{\xi}_i + \dfrac{1}{N}{}^i\hat{\boldsymbol{h}}_h \end{cases} \tag{35}$$

where $\gamma \in \mathbb{R}$ is a positive constant, $\boldsymbol{z}_i \in \mathbb{R}^p$ is an auxiliary state, and sign$(\cdot)$ *is the component-wise signum function. Then,*

- ${}^i\hat{\boldsymbol{h}}_h$ *approaches* $\boldsymbol{h}_h$ *in finite time* T_h, $\forall i = 1, ..., N$. *Equivalently, by defining the estimation error* ${}^i\tilde{\boldsymbol{h}}_h = \boldsymbol{h}_h - {}^i\hat{\boldsymbol{h}}_h$, *it approaches the origin in finite time* T_h.
- $\hat{\boldsymbol{h}}_{int,i}$ *approaches* $\boldsymbol{h}_{int,i}$ *in finite time* T_h, $\forall i = 1, ..., N$. *Equivalently, by defining the estimation error* $\tilde{\boldsymbol{h}}_{int,i} = \boldsymbol{h}_{int,i} - \hat{\boldsymbol{h}}_{int,i}$, *it approaches the origin approaches the origin in finite time.*

Proof By leveraging the same reasoning as in [32], it can be proved that the estimate ${}^i\hat{\boldsymbol{h}}_h$ converges to the average of $-N\boldsymbol{\xi}_i$ in finite-time T_h. Thus, by virtue of (34) and by recalling that, by construction, it holds $\sum_{i=1}^N \boldsymbol{h}_{int,i} = \boldsymbol{0}_p$, it follows ${}^i\hat{\boldsymbol{h}}_h \to -\frac{1}{N}\sum_{i=1}^N \boldsymbol{\xi}_i \approx \boldsymbol{h}_h$ or, equivalently, ${}^i\tilde{\boldsymbol{h}}_h \to \boldsymbol{0}_p$. Therefore, based on (34) and (35), the i th robot can also estimate its contribution to the internal wrenches $\boldsymbol{h}_{int,i}$ as follows

$$\hat{\boldsymbol{h}}_{int,i} = \boldsymbol{\xi}_i + \frac{1}{N}{}^i\hat{\boldsymbol{h}}_h \tag{36}$$

Since ${}^i\tilde{\boldsymbol{h}}_h \to 0$, from (34) it also holds

$$\hat{\boldsymbol{h}}_{int,i} \to \boldsymbol{\xi}_i + \frac{1}{N}\boldsymbol{h}_h = \boldsymbol{h}_{int,i} \tag{37}$$

This completes the proof.

Finally, as consequence of the lemma above, the wrench contribution of robot i to the object motion can be estimated as

$$\boldsymbol{h}_i - \hat{\boldsymbol{h}}_{int,i} = \boldsymbol{h}_i - \boldsymbol{\xi}_i - \frac{1}{N}{}^i\hat{\boldsymbol{h}}_h = \boldsymbol{\Gamma}_i \boldsymbol{G}^\dagger \boldsymbol{G}_i \boldsymbol{h}_i + \boldsymbol{\Gamma}_i \boldsymbol{G}^\dagger \boldsymbol{\theta}_i - \frac{1}{N}{}^i\hat{\boldsymbol{h}}_h \tag{38}$$

which converges to the actual value as well.

4.2 Generation and estimation of the object trajectory $\boldsymbol{x}_v$

Depending on the role of the i th robot, different approaches are pursued.

4.2.1 Leader robot

The leader robot is in charge of estimating the human model (Section 3.1) based on the estimate made as in (35) and defining the virtual input $\boldsymbol{u}_v$ (Section 3.2), from which the object reference trajectory is then derived as in (25).

4.2.2 Follower robot

In order for the followers to estimate the reference trajectory, the solution in [33] is exploited. Let us denote with $\boldsymbol{\chi}_v$ the stacked vector of the desired trajectory, that is $\boldsymbol{\chi}_v = \begin{bmatrix} \boldsymbol{x}_v{}^{\mathrm{T}} & \dot{\boldsymbol{x}}_v{}^{\mathrm{T}} & \ddot{\boldsymbol{x}}_v{}^{\mathrm{T}} \end{bmatrix}^T \in \mathbb{R}^{3p}$ and with ${}^i\hat{\boldsymbol{\chi}}_v$ the respective estimate made by the follower robot i. The following distributed observer is adopted by the followers

$$\begin{cases} {}^i\dot{\hat{\boldsymbol{\chi}}}_v = \boldsymbol{A}_\chi {}^i\hat{\boldsymbol{\chi}}_v - \mu_{v,1} \boldsymbol{B}_\chi \boldsymbol{B}_\chi^{\mathrm{T}} \boldsymbol{P}_\chi^{-1} {}^i\hat{\boldsymbol{\nu}}_v - \mu_{v,2} \mathrm{sign}\left(\boldsymbol{P}_\chi^{-1} {}^i\hat{\boldsymbol{\nu}}_v\right) \\ {}^i\hat{\boldsymbol{\nu}}_v = \sum_{j \in \mathcal{N}_i,\, j \neq l} \left({}^i\hat{\boldsymbol{\chi}}_v - {}^j\hat{\boldsymbol{\chi}}_v\right) + b_i \left({}^i\hat{\boldsymbol{\chi}}_v - \boldsymbol{\chi}_v\right) \end{cases} \tag{39}$$

where l is the index associated with the leader robot, i belongs to the set of the follower robots, b_i is 1 if the leader belongs to $\mathcal{N}_i$ and 0 otherwise, $\mu_{v,1}, \mu_{v,2} \in \mathbb{R}$ are positive gains, $\boldsymbol{A}_\chi \in \mathbb{R}^{3p \times 3p}$ and $\boldsymbol{B}_\chi \in \mathbb{R}^{3p}$ are matrices selected as

$$\boldsymbol{A}_\chi = \begin{bmatrix} \boldsymbol{O}_p & \boldsymbol{I}_p & \boldsymbol{O}_p \\ \boldsymbol{O}_p & \boldsymbol{O}_p & \boldsymbol{I}_p \\ \boldsymbol{O}_p & \boldsymbol{O}_p & \boldsymbol{O}_p \end{bmatrix}, \quad \boldsymbol{B}_\chi = \begin{bmatrix} \boldsymbol{O}_p & \boldsymbol{O}_p & \boldsymbol{I}_p \end{bmatrix}^T$$

and $\boldsymbol{P}_\chi \in \mathbb{R}^{3p \times 3p}$ is a positive definite matrix. By following the same reasoning as in [33], it can be proved that, under a proper selection of gains, the observer in (39) guarantees the finite-time leader tracking, i.e. it holds in finite-time T_χ

$$\| {}^i\hat{\boldsymbol{\chi}}_v(t) - \boldsymbol{\chi}_v(t) \| = 0 \, \forall i \neq l, \; t \geq T_\chi \tag{40}$$

4.3 Distributed low-level control

The control input $\boldsymbol{u}_i$ in (1) to cooperatively track the object reference trajectory and control the internal stresses, in the hypothesis of uncertain dynamics (2), is here devised. Let us denote with $\boldsymbol{e}_{int,i}$ the internal wrench error vector of robot i, i.e. $\boldsymbol{e}_{int,i} = \boldsymbol{h}^d_{int,i} - \boldsymbol{h}_{int,i} \in \mathbb{R}^p$, being $\boldsymbol{h}^d_{int,i} = \boldsymbol{\Gamma}_i \boldsymbol{h}^d_{int}$, and let us introduce the following integral error $\Delta\boldsymbol{u}_{f,i} \in \mathbb{R}^p$

$$\Delta\boldsymbol{u}_{f,i}(t) = k_f \int_{t_0}^{t} \boldsymbol{e}_{int,i}\, d\tau \tag{41}$$

with $k_f \in \mathbb{R}$ a positive scalar regulating the internal wrench control, and the error vector $\boldsymbol{e}_{x,i} \in \mathbb{R}^p$

$$\boldsymbol{e}_{x,i}(t) = ({}^i\hat{\boldsymbol{x}}_v - \boldsymbol{x}_i) + k_c \int_{t_0}^{t} \sum\nolimits_{j\in\mathcal{N}_i} (\boldsymbol{x}_j - \boldsymbol{x}_i) d\tau \tag{42}$$

with $k_c \in \mathbb{R}$ a positive constant, which is composed of a first term for the tracking of the object trajectory and a second synchronization term aimed at limiting the internal forces during the transient phases or due to unmodeled dynamics. Finally, let us introduce the following auxiliary variables

$$\begin{cases} \boldsymbol{\zeta}_i = {}^i\dot{\hat{\boldsymbol{x}}}_v + k_c \sum\nolimits_{j\in\mathcal{N}_i} (\boldsymbol{x}_j - \boldsymbol{x}_i) + k_p \boldsymbol{e}_{x,i} \quad \in \mathbb{R}^p \\ \tilde{\boldsymbol{\zeta}}_i = \boldsymbol{\zeta}_i - \dot{\boldsymbol{x}}_i = \dot{\boldsymbol{e}}_{x,i} + k_p \boldsymbol{e}_{x,i} \quad \in \mathbb{R}^p \\ \boldsymbol{\rho}_i = \boldsymbol{\zeta}_i + \Delta\boldsymbol{u}_{f,i} \quad \in \mathbb{R}^p \\ \boldsymbol{s}_i = \tilde{\boldsymbol{\zeta}}_i + \Delta\boldsymbol{u}_{f,i} \quad \in \mathbb{R}^p \end{cases} \tag{43}$$

with $k_p \in \mathbb{R}$ a positive constant and $\hat{\Delta}\boldsymbol{u}_{f,i}$ the estimate of $\Delta\boldsymbol{u}_{f,i}(t)$ made by robot i as

$$\hat{\Delta}\boldsymbol{u}_{f,i}(t) = k_f \int_{t_0}^{t} \hat{\boldsymbol{e}}_{int,i}\, d\tau \tag{44}$$

where $\hat{\boldsymbol{e}}_{int,i} = \boldsymbol{h}^d_{int,i} - \hat{\boldsymbol{h}}_{int,i}$ which takes into account that the internal wrench $\boldsymbol{h}_{int,i}$ is not known but only locally estimated as in (37). By extending the approach in [21], the following control law is proposed

$$\boldsymbol{u}_i = \hat{\boldsymbol{M}}_i \dot{\boldsymbol{\rho}}_i + \hat{\boldsymbol{C}}_i \boldsymbol{\rho}_i + \hat{\boldsymbol{\eta}}_i + \boldsymbol{K}_s \boldsymbol{s}_i + \Delta\boldsymbol{u}_i = \boldsymbol{Y}_i(\boldsymbol{x}_i, \dot{\boldsymbol{x}}_i, \boldsymbol{\rho}_i, \dot{\boldsymbol{\rho}}_i)\hat{\boldsymbol{\pi}}_i + \boldsymbol{K}_s \boldsymbol{s}_i + \Delta\boldsymbol{u}_i \tag{45}$$

being $\boldsymbol{K}_s \in \mathbb{R}^{p\times p}$ a positive definite matrix and $\Delta\boldsymbol{u}_i \in \mathbb{R}^p$ selected as

$$\begin{aligned} \Delta\boldsymbol{u}_i =& \kappa_i(t)\boldsymbol{s}_i + \boldsymbol{h}^d_{int,i} + \hat{\Delta}\boldsymbol{u}_{f,i} + \boldsymbol{\Gamma}_i \boldsymbol{G}^\dagger \boldsymbol{G}_i \boldsymbol{h}_i + \boldsymbol{\Gamma}_i \boldsymbol{G}^\dagger \boldsymbol{\theta}_i - \frac{1}{N}\, {}^i\hat{\boldsymbol{h}}_h \\ =& \underbrace{\kappa_i(t)\boldsymbol{s}_i}_{a} + \underbrace{\boldsymbol{h}^d_{int,i} + \hat{\Delta}\boldsymbol{u}_{f,i}}_{b} + \underbrace{\boldsymbol{\Gamma}_i \boldsymbol{G}^\dagger \boldsymbol{G}_i \boldsymbol{h}_i + \boldsymbol{\Gamma}_i \boldsymbol{G}^\dagger \boldsymbol{\theta}_i - \frac{1}{N}\boldsymbol{h}_h + \frac{1}{N}\, {}^i\tilde{\boldsymbol{h}}_h}_{c} \end{aligned} \tag{46}$$

with $\kappa_i(t) \in \mathbb{R}$ a positive time-varying gain, and where

- a) is a robust term to guarantee convergence of internal forces in the transient phase and despite model uncertainties;
- b) is a force feed-forward and integral error contribution;
- c) represents, based on (38), the compensation of the contribution to the external generalized forces made by robot i on the object.

Moreover, the dynamic parameters of robot i are updated as

$$\dot{\hat{\boldsymbol{\pi}}}_i = \boldsymbol{K}_\pi^{-1} \boldsymbol{Y}_i^{\mathrm{T}}(\boldsymbol{x}_i, \dot{\boldsymbol{x}}_i, \boldsymbol{\rho}_i, \dot{\boldsymbol{\rho}}_i)^{\mathrm{T}} \boldsymbol{s}_i \tag{47}$$

with $\boldsymbol{K}_\pi \in \mathbb{R}^{n_{\pi_i} \times n_{\pi_i}}$ a positive definite matrix.
The analysis of control law $\boldsymbol{u}_i$ is provided in the theorem.

Theorem 1 *Let us consider N robots with dynamics in* (1) *for which an estimate is known as in* (2)*. Let us consider the observer in* (39)*, the control law in* (45) *and the parameters update law in* (47)*. Then, it asymptotically holds $\boldsymbol{x}_i \to \boldsymbol{x}_v$ and $\boldsymbol{e}_{int,i} \to \boldsymbol{0}_p$ $\forall i = 1, ..., N$.*

Proof The proof is provided in the Appendix.

5 Simulation results

Table 2 Simulation parameters.

Parameter	Value	Parameter	Value
$\boldsymbol{M}_v$ (eq. (8))	$\mathrm{diag}\{2\boldsymbol{I}_3\mathrm{kg}, \boldsymbol{I}_3\mathrm{kgm}^2\}$	$\bar{e}$ (eq.(17))	0.5
$\boldsymbol{D}_v$ (eq. (18))	$\mathrm{diag}\{10\boldsymbol{I}_3\mathrm{Ns/m}, 8\boldsymbol{I}_3\mathrm{Nms}\}$	T (eq.(17))	0.001s
$\boldsymbol{K}_\gamma$ (eq. (19))	$0.3\boldsymbol{I}_6$	Δ (eq.(17))	0.2s
t_h (eq. (19))	1	$\boldsymbol{K}_\theta$ (eq. (28))	$800\boldsymbol{I}_6$
$\boldsymbol{R}_h$ (eq. (9))	$0.5\boldsymbol{I}_3$	γ (eq. (35))	300
$\boldsymbol{R}_v$ (eq. (9))	$0.1\boldsymbol{I}_6$	$\mu_{v,1}$ (eq. (39))	30
$\boldsymbol{Q}_{r,d}$ (eq. (9))	$10\,\mathrm{diag}\{250\boldsymbol{I}_3, \boldsymbol{I}_3, 250\boldsymbol{I}_3, \boldsymbol{I}_3\}$	k_f (eq. (41))	0.5
$\boldsymbol{W}_{h,d}$ (eq. (10))	$\boldsymbol{I}_6$	$\mu_{v,2}$ (eq. (39))	25
λ (eq.(15))	0.998	k_c (eq. (42))	1
$\boldsymbol{P}_0$ (eq.(15))	$10000\boldsymbol{I}_9$	k_p (eq. (43))	1
α (eq. (16))	0.1	$\boldsymbol{K}_s$ (eq. (45))	1

In this section, results are provided to validate the proposed approach. Matlab[1] environment was adopted to corroborate the theoretical findings in which both modelling and control were implemented. Moreover, CoppeliaSim[2]

[1] `http://www.mathworks.com`
[2] `http://www.coppeliarobotics.com`

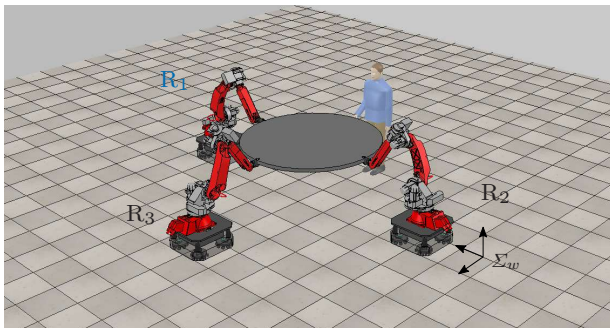

Fig. 4 Simulation setup composed of 3 cooperative robots (R_i, $i = 1, 2, 3$) rigidly grasping an object with which a human operator physically interacts; the leader robot (R_1) is highlighted with blue color and the world reference frame Σ_w is reported.

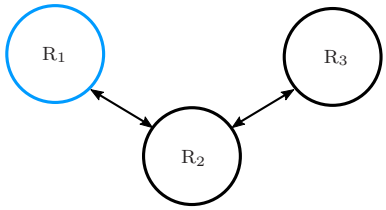

Fig. 5 Communication graph. Leader robot is highlighted with a blue node.

was adopted to visualize the robots and human motion as in Figure 4; the respective environment is provided at the link[3]. In detail, the setup shown in the figure is composed of $N = 3$ Comau Smart SiX manipulators (6 DOFs) mounted on mobile bases (2 DOFs) and they rigidly grasp a cylindrical object. Robots are redundant and it holds $p = 6$ and $m = 3$ in Table 1; moreover, the reduced regressor matrix $\boldsymbol{Y}_i \in \mathbb{R}^{6\times 56}$ ($n_{\pi_i} = 56$) in (1) is considered and a uniformly distributed 5% uncertainty is assumed concerning the robots' dynamic parameters $\boldsymbol{\pi}_i$, $i = 1, 2, 3$. For the sake of the implementation on a real setup, an initial estimation of the robot dynamic model might be obtained by resorting to one of the approaches mentioned in [34]. Furthermore, it is also required the robots agree on a common reference frame in which the object trajectory and the estimation of global variables are specified and/or computed. However, this requirement is common to almost all distributed algorithms and, in the case of mobile manipulators, implies the robots to be able to localize in a common frame; this can be obtained, for example, by using passive markers to be detected by on-board vision sensors. The latter can also be used to estimate the point in which the object is grasped by the human operator if such an information is not known beforehand.
Concerning the communication graph, shown in Figure 5, bi-directional communication links are considered between robots 1 and 2 and between robots 2 and 3, while robot 1, for example, is set as leader. Finally, the manipulated object is represented by a cylinder with mass $m_o = 5$ kg, radius $r_o = 1$ m

[3] `http://webuser.unicas.it/lai/robotica/papers/JINTVREPscene.ttt`

and height $h_o = 0.05$ m. In order to simulate the overall system dynamics, the Udwadia-Kalaba equation of motion for constrained systems is adopted which, as done in [35], allows to compute the constraint wrenches $\boldsymbol{h}$ arising from the robots rigid grasping constraint. In addition, uncertainty on both the manipulated object model and initial human parameters is introduced. In particular, for each robot, a uniformly distributed 3% of error is generated regarding the object dynamic model, while, concerning the initial human parameters, an uncertainty with normal distribution $\mathcal{N}(0, 0.3\pi_{h,i})\,\forall i \in \{1, ..., 9\}$, with $\pi_{h,i}$ the i th element of vector $\boldsymbol{\pi}_h$ in (4), is introduced.
The objective of the simulation is to achieve the shared control of the object motion where, as shown in Figure 6, the robots task is to perform a circular trajectory in xy-plane with radius $r_c = 1.5$ m, center $\boldsymbol{c} = [0\ 0\ 0.94]^{\mathrm{T}}$m and period $T_c = 3.8$ s, while keeping the orientation constant, whereas the human desired configuration coincides with the circumference center, i.e. $\boldsymbol{p}_{h,d} \equiv \boldsymbol{c}$. Note that, as assumed for example in [36], a constant human desired motion is typically considered for human reaching motions. The human operator force is modeled according to eq. (3) where stiffness $\boldsymbol{K}_h$ and damping $\boldsymbol{D}_h$ matrices are increased during the simulation time (as discussed below and shown in Figure 7 with solid lines) in order to dynamically modify the object trajectory and make the human leading the motion. Finally, zero internal wrenches are required, i.e. the stacked vector of the desired internal wrenches $\boldsymbol{h}^d_{int} = [\boldsymbol{h}^{d\ \mathrm{T}}_{int,1}\ \boldsymbol{h}^{d\ \mathrm{T}}_{int,2}\ \boldsymbol{h}^{d\ \mathrm{T}}_{int,3}]^{\mathrm{T}} \in \mathbb{R}^{18}$ is $\boldsymbol{h}^d_{int} = \boldsymbol{0}_{18}$.

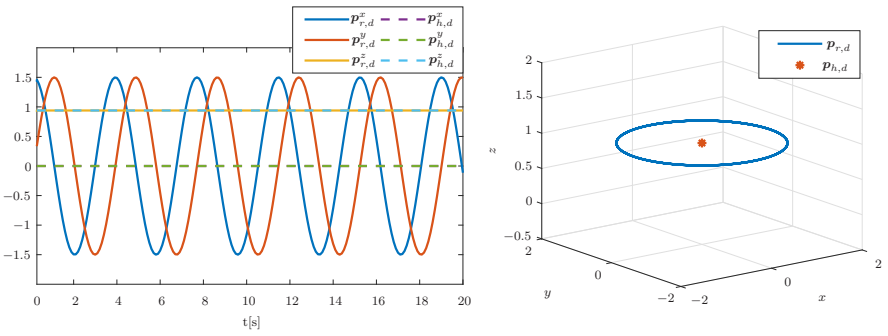

Fig. 6 Representation in 2D (left) and 3D (right) of the robots' desired position (solid lines on the left and blue line on the right) and the human desired one (dashed lines on the left and red star on the right).

A summary video of the simulation results is available at the link[4], while simulation parameters are reported in Table 2. Among them and concerning the human parameters estimation discussed in Section 3.1, the initial covariance matrix $\boldsymbol{P}_0$ is set to a high value to denote a high uncertainty on the initial human parameters, while the values of T and Δ are selected as in [18]. In addition, the values of the weighting matrix $\boldsymbol{Q}_{r,d}$ are defined so as to make the

[4] https://youtu.be/eQwBT74F1Po

contribution associated with the robots desired trajectory comparable with respect to the one associated to the human operator. Finally, the rationale behind the gain matrix $\boldsymbol{K}_\theta$ is, as also stressed in Remark 2, to set it to a higher value than the low-level control law gains in order to estimate the respective quantity sufficiently fast. The same reasoning applies for the choice of the gain γ.

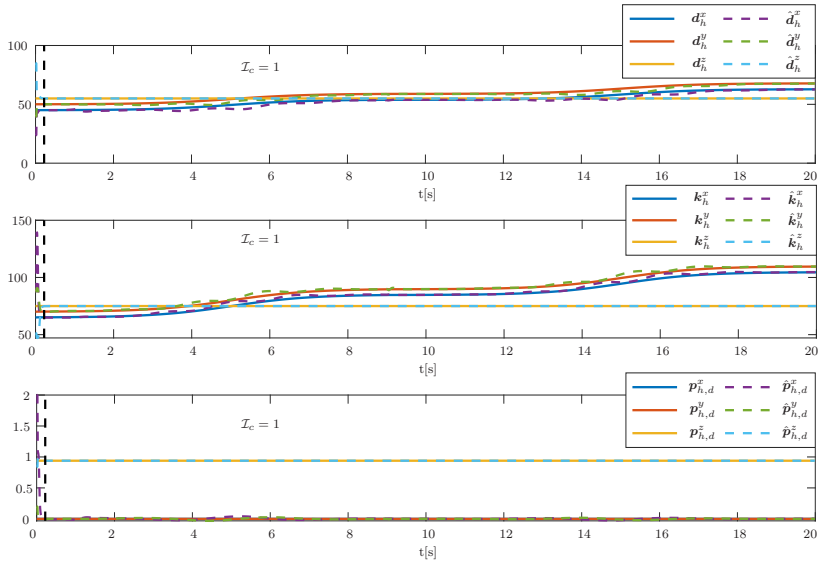

Fig. 7 Evolution of the human parameters $\boldsymbol{d}_h$, $\boldsymbol{k}_h$ and $\boldsymbol{p}_{h,d}$ (from the top, solid lines), respectively, along x, y and z directions and the respective estimates (dashed lines); the time instant $t_c \approx 0.22$ s in which the confidence index $\mathcal{I}_c$ in (17) becomes 1 is highlighted by the black vertical line.

Simulation results are reported in Figures 7-16. More specifically, Figure 7 shows the evolution of the human parameters (solid lines) along x, y and z directions as well as the respective estimates (dashed lines) computed by the leader robot. In particular, the human stiffness $\boldsymbol{K}_h$ (middle plot) increases along x and y during the time intervals $[2, 8]$ s and $[12, 18]$ s in order to increase the leading action of the human. Similarly, an increase of the human damping (top plot) is simulated during the same intervals as a stabilizing and slowing down action. In addition, the time instant $t_c \approx 0.22$s in which the estimate is assessed reliable according to the confidence index in (17) is highlighted (vertical black line).

Figure 8 reports the position components $\boldsymbol{p}_v$ of the desired object trajectory (solid bold lines) resulting from the devised strategy (orientation variables are constant). In particular, as long as the estimate is considered not reliable ($t < t_c$), the desired object motion is generated according to the admittance model in (18) and is driven towards the desired position of the human; then, starting

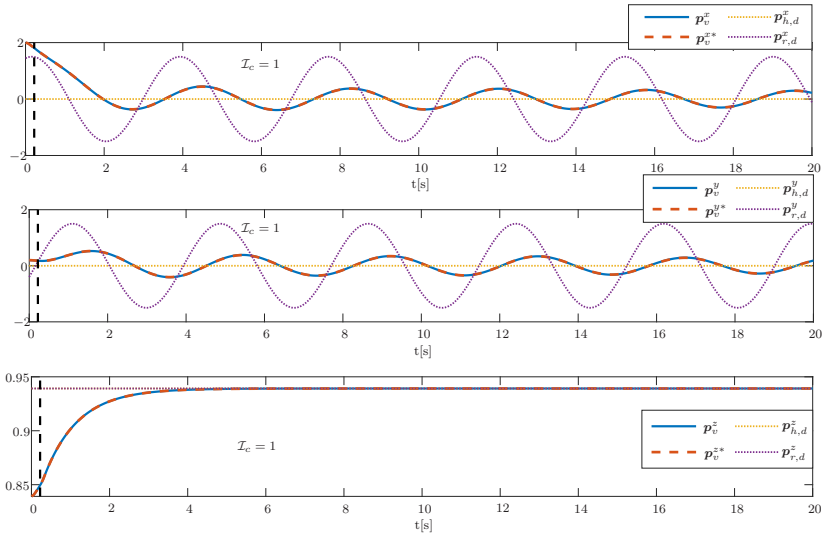

Fig. 8 Evolution of the position of the virtual model (blue solid lines) along x, y and z directions compared with the ideal one obtained with the real human parameters $\boldsymbol{\pi}_h$ (red dashed lines); for the sake of completeness, human (yellow dotted lines) and robot (purple dotted lines) desired positions and time instant when it holds $\mathcal{I}_c = 1$ (black line) are also shown.

from time t_c, the optimal policy in (11) for the shared control is adopted which leads to perform a circular trajectory with time-varying radius ($< r_c$) and time-varying period ($< T_c$). In detail, the trajectory dynamically adapts according to the human behavior: the higher the human stiffness, the more the motion amplitudes reduce, being the human desired position coincident with the center of the trajectory, i.e. $\boldsymbol{p}_{h,d} = [0\ 0\ 0.94]^{\mathrm{T}}$ m, as also reported in the figure (yellow dotted lines); moreover, the higher the human damping, the slower the resulting motion is. For the sake of comparison, the robots desired position $\boldsymbol{p}_{r,d}$ is also shown in the figure (purple dotted lines). In addition, in order to show the effect of human arm parameter estimation on the overall behavior of the system, the object trajectory obtained in the ideal case of zero human parameter estimation error, i.e. with $\boldsymbol{\pi}_h = \hat{\boldsymbol{\pi}}_h$, is reported (dashed line, denoted with $\boldsymbol{p}_v^*$) and is shown to be equivalent to the one derived with the estimated parameters in Figure 7.

Figure 9 (top plot) shows the error $\|{}^l\hat{\boldsymbol{h}}_h - \boldsymbol{h}_h\|$ between the real human wrench $\boldsymbol{h}_h$ and the one estimated according to Lemma 2. The figure shows that the estimated wrench converges to the real one and in finite time according to the theory. Therefore, each agent is adopting a consistent estimate for computing the local control strategy. In the same way, the bottom plot shows that the internal wrench $\boldsymbol{h}_{int}$ converges to the desired value $\boldsymbol{h}_{int}^d$ since the error $\|\boldsymbol{h}_{int} - \boldsymbol{h}_{int}^d\|$ converges to the origin and required in Problem 1. A zoom of the evolution of both quantities up to 0.05 s is provided in the plots.

The purpose of Figure 10 is to show the performance of the two-layer architecture presented in Figure 2. As explained in previous sections, the high-level is in charge of defining the object reference trajectory $\boldsymbol{x}_v$ which is the solution of the optimal problem defined in (9). This trajectory represents the desired trajectory of the object $\boldsymbol{x}_o$ to be tracked by the robots. Therefore, Figure 2 shows that the position $\|\boldsymbol{x}_v - \boldsymbol{x}_o\|$ (top) and velocity $\|\dot{\boldsymbol{x}}_v - \dot{\boldsymbol{x}}_o\|$ (bottom) tracking errors converge to the origin, which means that the real object trajectory converges to the desired one.

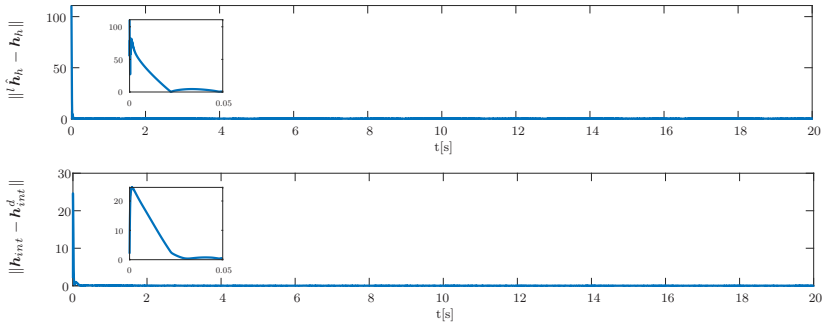

Fig. 9 Evolution of the human forces estimation error (top) and of the internal forces error (bottom).

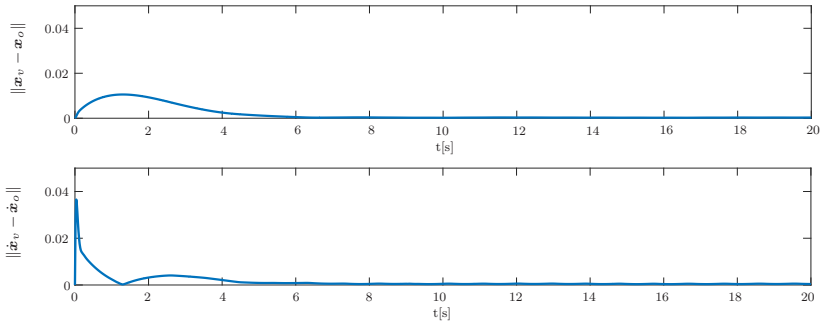

Fig. 10 Evolution of trajectory tracking error $\|\boldsymbol{x}_v - \boldsymbol{x}_o\|$ (top) and its derivative $\|\dot{\boldsymbol{x}}_v - \dot{\boldsymbol{x}}_o\|$ (bottom).

Finally, the effects of some main parameters of the framework have been analyzed. More specifically, the influence of the weight matrices $\boldsymbol{Q}_{r,d}$ and $\boldsymbol{R}_v$ in the cost function (9) as well as the inertia matrix $\boldsymbol{M}_v$ of the virtual model (8) has been considered. No plot of the internal wrench is provided in the following analysis since it is not affected by the considered matrices and for the sake of space.

Concerning the weight matrices $\boldsymbol{Q}_{r,d}$, it regulates how much relevance is given

to tracking the robots trajectory and its effect has been investigated in regard to the resulting shared motion and human force. In particular, by expressing $\boldsymbol{Q}_{r,d}$ as $\boldsymbol{Q}_{r,d} = \text{diag}\{Q_{r,p}\boldsymbol{I}_3, Q_{r,o}\boldsymbol{I}_3, Q_{r,p}\boldsymbol{I}_3, Q_{r,o}\boldsymbol{I}_3\}$, Figures 11 and 12 report the object motion and human force, respectively, obtained by varying $Q_{r,p}$ in the set $\{10, 500, 2500, 10000\}$. For the sake of comparison, the human desired motion (dotted orange line) and the robots desired one (dotted gray line) are also shown in Figure 11. The figures make evident that, as the weight $Q_{r,p}$ decreases, the resulting object trajectory approaches the human desired configuration $\boldsymbol{p}_{h,d}$, and, accordingly, the human effort decreases since the person lead the control. On the contrary, the higher the value, the more the resulting trajectory gets closer to the robots desired circular motion, thus leading to a major human effort. It follows that the role of human and robots in the shared control is driven both by the tuning of the static weighting matrices in the cost function, such as $\boldsymbol{Q}_{r,d}$, and, dynamically, by the time-varying parameters of the human arm. No analysis of the weight matrices $\boldsymbol{Q}_{h,d}$ and $\boldsymbol{R}_h$ has been reported since their effect is dual to the one of $\boldsymbol{Q}_{r,d}$, i.e. the higher norm the more the human desired trajectory is pursued with respect to the robot one and the human force minimized.

As far as the weight $\boldsymbol{R}_v$ is concerned, it regulates how much relevance is given to the minimization of the robots effort $\boldsymbol{u}_i$. Figures 13 and 14 report the norm of the overall robot efforts and the resulting object motion, respectively, when varying R_v. More specifically, by denoting with $\boldsymbol{u} = [\boldsymbol{u}_1^{\mathrm{T}}\ \boldsymbol{u}_2^{\mathrm{T}}\ \cdots \boldsymbol{u}_N^{\mathrm{T}}]^{\mathrm{T}} \in \mathbb{R}^{Np}$ the stacked vector of the robots inputs, Figure 13 shows how by increasing the weight R_v, the robots control effort, i.e. $\|\boldsymbol{u}\|$, reduces. This is achieved, as reported in Figures 14, by slowing down the trajectory and by decreasing the amplitude of the oscillations. It thus follows that the higher R_v the more the control effort is reduced at the expense of lower tracking performance of the desired robot trajectory. As for the previous parameters, the human desired motion (dotted orange line) and the robots desired one (dotted gray line) are also shown in Figure 14 for the sake of completeness. Note that the same trajectory is recorded for all parameters for $t < t_c$ since the weight matrices are only used in the cost function and do not affect the admittance controller in eq. (18) that is used when the human estimation is not reliable.

Regarding the inertia matrix, let us formulate it as $\boldsymbol{M}_v = \text{diag}\{M_{v,p}\boldsymbol{I}_3, M_{v,o}\boldsymbol{I}_3\}$. The following set of values matrix has been tested for analyzing its influence: $M_{v,p} = \{2, 5, 10, 50, 500\}$. Figures 15 and 16 report the resulting object motion and the norm of the overall robots' effort, respectively, when varying $M_{v,p}$. In particular, the latter influences the bandwidth of the virtual dynamics implying that the higher $M_{v,p}$ the slower the system's response will be. This behavior is evident from the figures where a more dampened motion (see Figure 15), with reduced acceleration, is obtained as $M_{v,p}$ grows. This also implies that a lower robots control effort is required when increasing $M_{v,p}$.

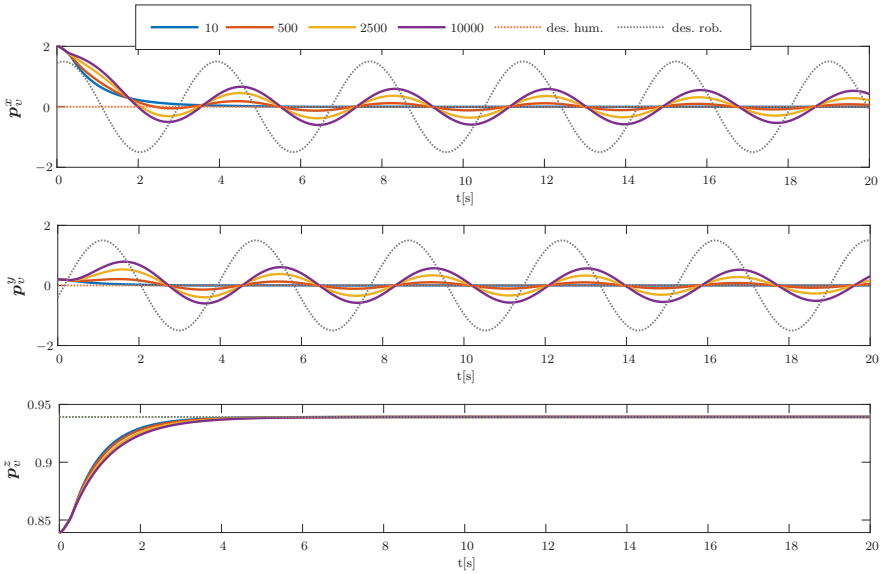

Fig. 11 Evolution of the object motion (bold lines) along x, y and z directions by varying the robots weight $Q_{r,p} \in \{10, 500, 2500, 10000\}$ in the cost function. The human desired motion (dotted orange line) and the robots desired one (dotted gray line) are also shown.

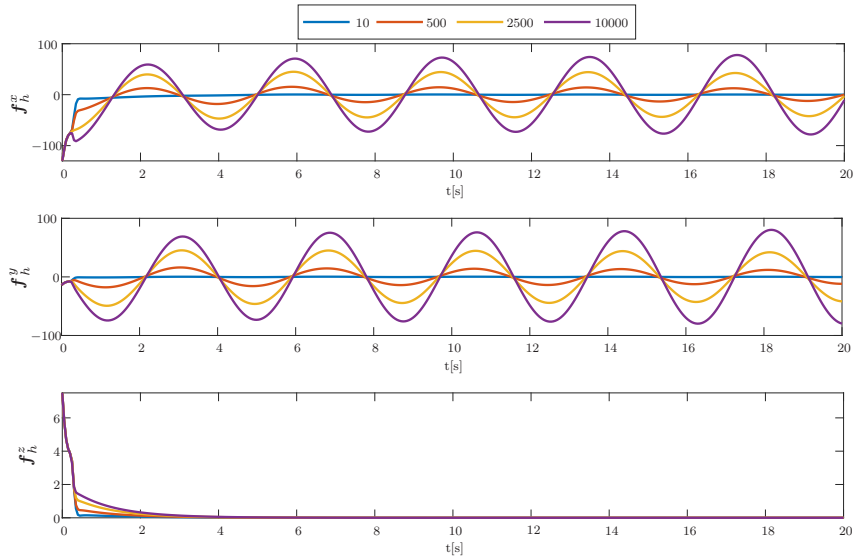

Fig. 12 Evolution of the human force along x, y and z directions by varying the robots weight $Q_{r,p} \in \{10, 500, 2500, 10000\}$ in the cost function.

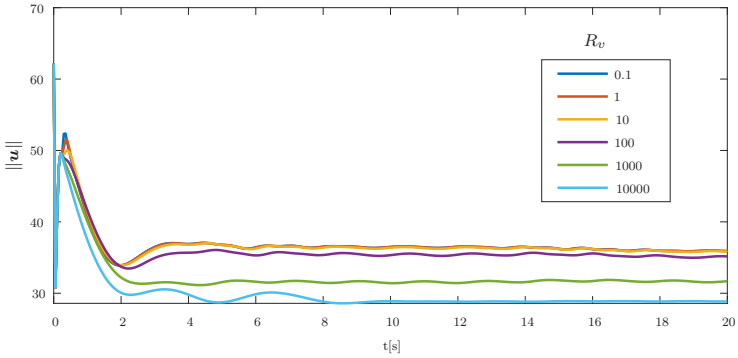

Fig. 13 Evolution of the norm of the overall robots control input by varying the robots effort weight $R_v \in \{0.1, 1, 10, 100, 1000, 10000\}$ in the cost function.

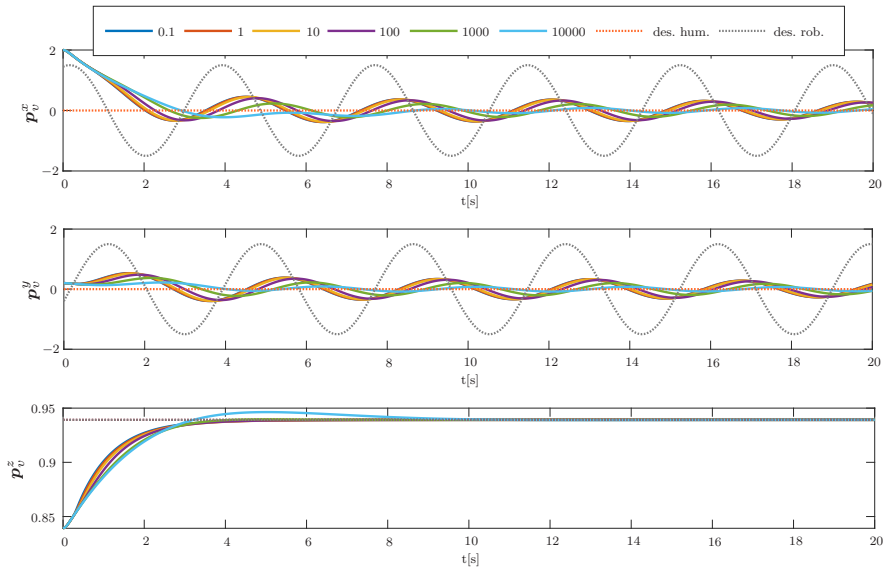

Fig. 14 Evolution of the object motion along x, y and z directions by varying the robots effort weight $R_v \in \{0.1, 1, 10, 100, 1000, 10000\}$ in the cost function. The human desired motion (dotted orange line) and the robots desired one (dotted gray line) are also shown.

6 Conclusions

In this paper, a general framework to allow a human operator to physically interact with a multi-manipulator system in a distributed setting has been proposed. In the devised solution, a virtual dynamics for the manipulated object has been set whose input is the solution of a LQT problem. In the latter, both human and robots tasks have been taken into account, with former estimated, for instance, via RLS. The optimal object trajectory is then

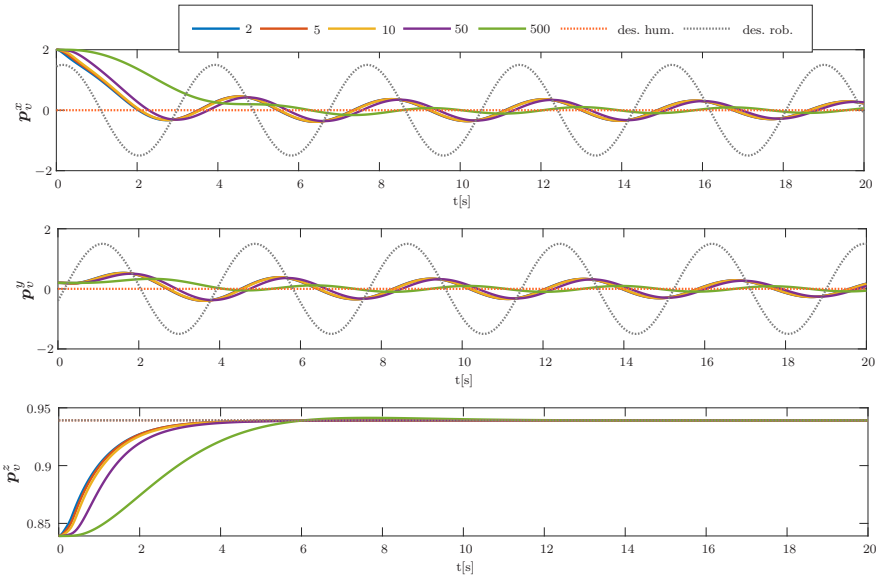

Fig. 15 Evolution of the object motion along x, y and z directions by varying the virtual inertia $M_{v,p}$. The human desired motion (dotted orange line) and the robots desired one (dotted gray line) are also shown.

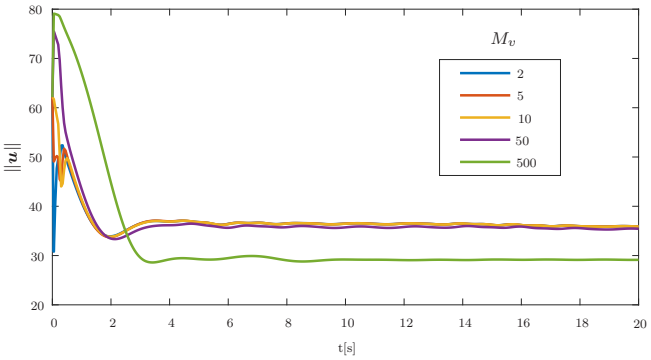

Fig. 16 Evolution of the norm of the robots control input by varying the virtual inertia $M_{v,p}$.

tracked by robots via a time-varying gain distributed adaptive control that takes into account several sources of uncertainty. As future work, constraint optimal control strategies will be adopted at the top level to take into consideration robot constraints [37]. Moreover, the overall approach only takes into consideration the human interaction wrench, robot and human's desired trajectory; the overall approach might be modified so as to take into consideration

also the ergonomics of the interaction. Finally, experiments will be carried out on a real platform composed of two dual-arm Kinova Movo robots[5].

7 Appendix

To prove Theorem 1, let us first derive the closed loop dynamics or robot i. By folding (45) in (1), it holds

$$\boldsymbol{M}_i\dot{\boldsymbol{s}}_i = -\boldsymbol{C}_i\boldsymbol{s}_i - \boldsymbol{K}_s\boldsymbol{s}_i - \Delta\boldsymbol{u}_i + \boldsymbol{h}_i + \boldsymbol{Y}_i(\boldsymbol{x}_i, \dot{\boldsymbol{x}}_i, \boldsymbol{\rho}_i, \dot{\boldsymbol{\rho}}_i)\tilde{\boldsymbol{\pi}}_i \tag{48}$$

Now, let us consider the following Lyapunov function

$$V = \frac{1}{2}\sum_{i=1}^{N}\left(\boldsymbol{s}_i^{\mathrm{T}}\boldsymbol{M}_i\boldsymbol{s}_i + \frac{1}{k_f}\hat{\Delta}\boldsymbol{u}_{f,i}^{\mathrm{T}}\hat{\Delta}\boldsymbol{u}_{f,i} + \tilde{\boldsymbol{\pi}}_i^{\mathrm{T}}\boldsymbol{K}_\pi\tilde{\boldsymbol{\pi}}_i\right) \tag{49}$$

By virtue of (48) and Property 1, the time derivative of V is

$$\begin{aligned}
\dot{V} &= \sum_{i=1}^{N}\Big(\boldsymbol{s}_i^{\mathrm{T}}\boldsymbol{M}_i\dot{\boldsymbol{s}}_i + \frac{1}{2}\boldsymbol{s}_i^{\mathrm{T}}\dot{\boldsymbol{M}}_i\boldsymbol{s}_i + \hat{\Delta}\boldsymbol{u}_{f,i}^{\mathrm{T}}\tilde{\boldsymbol{h}}_{int,i} - \tilde{\boldsymbol{\pi}}_i^{\mathrm{T}}\boldsymbol{K}_\pi\dot{\tilde{\boldsymbol{\pi}}}_i\Big) \\
&= \sum_{i=1}^{N}\Big(-\boldsymbol{s}_i^{\mathrm{T}}\boldsymbol{K}_s\boldsymbol{s}_i + \frac{1}{2}(\dot{\boldsymbol{M}}_i - 2\boldsymbol{C}_i)\boldsymbol{s}_i + \boldsymbol{s}_i^{\mathrm{T}}(\boldsymbol{h}_i - \Delta\boldsymbol{u}_i) \\
&\quad + \hat{\Delta}\boldsymbol{u}_{f,i}^{\mathrm{T}}\tilde{\boldsymbol{h}}_{int,i} - \tilde{\boldsymbol{\pi}}_i^{\mathrm{T}}(\boldsymbol{K}_\pi\dot{\tilde{\boldsymbol{\pi}}}_i - \boldsymbol{Y}_i^{\mathrm{T}}(\boldsymbol{x}_i, \dot{\boldsymbol{x}}_i, \boldsymbol{\rho}_i, \dot{\boldsymbol{\rho}}_i)\boldsymbol{s}_i)\Big) \\
&= \sum_{i=1}^{N}\Big(-\boldsymbol{s}_i^{\mathrm{T}}\boldsymbol{K}_s\boldsymbol{s}_i + \hat{\Delta}\boldsymbol{u}_{f,i}^{\mathrm{T}}\tilde{\boldsymbol{h}}_{int,i} - \boldsymbol{s}_i^{\mathrm{T}}(\boldsymbol{e}_{int,i} + k_f\hat{\Delta}\boldsymbol{u}_{f,i} + \frac{1}{N}{}^i\tilde{\boldsymbol{h}}_h) \\
&\quad - \kappa_i(t)\boldsymbol{s}_i^{\mathrm{T}}\boldsymbol{s}_i - \tilde{\boldsymbol{\pi}}_i^{\mathrm{T}}(\boldsymbol{K}_\pi\dot{\tilde{\boldsymbol{\pi}}}_i - \boldsymbol{Y}_i^{\mathrm{T}}(\boldsymbol{x}_i, \dot{\boldsymbol{x}}_i, \boldsymbol{\rho}_i, \dot{\boldsymbol{\rho}}_i)\boldsymbol{s}_i)\Big)
\end{aligned} \tag{50}$$

Given the parameters update law in (47), (50) simplifies to

$$\begin{aligned}
\dot{V} = \sum_{i=1}^{N}\Big(&-\boldsymbol{s}_i^{\mathrm{T}}\boldsymbol{K}_s\boldsymbol{s}_i + \hat{\Delta}\boldsymbol{u}_{f,i}^{\mathrm{T}}\tilde{\boldsymbol{h}}_{int,i} - \kappa_i(t)\|\boldsymbol{s}_i\|^2 \\
&- (\tilde{\boldsymbol{\zeta}}_i + \hat{\Delta}\boldsymbol{u}_{f,i})^{\mathrm{T}}(\tilde{\boldsymbol{h}}_{int,i} + \hat{\Delta}\boldsymbol{u}_{f,i}) + \frac{1}{N}\boldsymbol{s}_i^{\mathrm{T}\,i}\tilde{\boldsymbol{h}}_h\Big)
\end{aligned} \tag{51}$$

Thus, by choosing

$$\kappa_i(t) > \frac{\|\tilde{\boldsymbol{\zeta}}_i\|}{\|\boldsymbol{s}_i\|^2}\|\tilde{\boldsymbol{h}}_{int,i} + \hat{\Delta}\boldsymbol{u}_{f,i}\|$$

it holds

$$\dot{V} \leq \sum_{i=1}^{N}\big(-\boldsymbol{s}_i^{\mathrm{T}}\boldsymbol{K}_s\boldsymbol{s}_i - \hat{\Delta}\boldsymbol{u}_{f,i}^{\mathrm{T}}\hat{\Delta}\boldsymbol{u}_{f,i} + \frac{1}{N}\|\boldsymbol{s}_i^{\mathrm{T}\,i}\|\|\tilde{\boldsymbol{h}}_h\|\big)$$

[5] www.kinovarobotics.com/en/products/mobile-manipulators

From Lemma 2, $\|\tilde{\boldsymbol{h}}_h\|$ converges to the origin after a finite time T_h; then after this time it holds

$$\dot{V} \leq \sum_{i=1}^{N} \big(- \boldsymbol{s}_i^{\mathrm{T}} \boldsymbol{K}_s \boldsymbol{s}_i - {}^i\hat{\Delta}\boldsymbol{u}_{f,i}^{\mathrm{T}} {}^i\hat{\Delta}\boldsymbol{u}_{f,i} \big)$$

which implies that $\dot{V}$ is semi-negative definite and, consequently, that V is bounded. By leveraging the boundedness of V and, then, of $\boldsymbol{s}_i$, $\hat{\Delta}\boldsymbol{u}_{f,i}$ and $\tilde{\boldsymbol{\pi}}_i$, it can be easily shown the $\ddot{V}$ is bounded as well. Thus, by virtue of Barbalat's lemma, $\dot{V}$ is uniformly continuous and converges to the origin, as well as $\boldsymbol{s}_i$ and $\hat{\Delta}\boldsymbol{u}_{f,i} = k_f \int_{t_0}^{t} \tilde{\boldsymbol{h}}_{int,i}\, d\tau$ (and, therefore, by definition $\tilde{\boldsymbol{h}}_{int,i}$). The main implication of the latter is that, since because of Lemma 2, $\tilde{\boldsymbol{h}}_{int,i}$ converges to the origin in finite time (that is the internal wrenches estimated via observer converges to the real one), then also $\boldsymbol{e}_{int,i}$, $\forall\, i$, converges to the origin.

In view of the expression of $\boldsymbol{s}_i$ in (43) and since $\hat{\Delta}\boldsymbol{u}_{f,i}$ converges to the origin, it follows

$$\dot{\boldsymbol{e}}_{x,i} + k_p \boldsymbol{e}_{x,i} = -\hat{\Delta}\boldsymbol{u}_{f,i}$$

which represents an asymptotically stable system (in the state variable $\boldsymbol{e}_{x,i}$) with vanishing input $-\hat{\Delta}\boldsymbol{u}_{f,i}$. Therefore, $\boldsymbol{e}_{x,i}$ asymptotically converges to the origin. Based on the expression of $\boldsymbol{e}_{x,i}$ in (42), it asymptotically holds

$$({}^i\hat{\boldsymbol{x}}_v - \boldsymbol{x}_i) + k_c \int_{t_0}^{t} \sum_{j \in \mathcal{N}_i} (\boldsymbol{x}_j - \boldsymbol{x}_i) d\tau \to \boldsymbol{0}_p \tag{52}$$

Let us now introduce the object trajectory estimate error ${}^i\tilde{\boldsymbol{x}}_v = \boldsymbol{x}_v - {}^i\hat{\boldsymbol{x}}_v \in \mathbb{R}^p$ and the object trajectory tracking error $\boldsymbol{e}_{v,i} = \boldsymbol{x}_v - \boldsymbol{x}_i \in \mathbb{R}^p$. From (52), it asymptotically holds

$$(\boldsymbol{x}_v - \boldsymbol{x}_i) + k_c \int_{t_0}^{t} \sum_{j \in \mathcal{N}_i} (\boldsymbol{x}_j - \boldsymbol{x}_v - \boldsymbol{x}_i + \boldsymbol{x}_v) d\tau = -{}^i\tilde{\boldsymbol{x}}_v$$

which can be rewritten as

$$\boldsymbol{e}_{v,i} + k_c \int_{t_0}^{t} \sum_{j \in \mathcal{N}_i} (-\boldsymbol{e}_{v,j} + \boldsymbol{e}_{v,i}) d\tau = -{}^i\tilde{\boldsymbol{x}}_v \tag{53}$$

By denoting with $\tilde{\boldsymbol{x}}_v \in \mathbb{R}^{Np}$ and $\boldsymbol{e}_v \in \mathbb{R}^{Np}$ the stacked vectors of the errors ${}^i\tilde{\boldsymbol{x}}_v$ and $\boldsymbol{e}_{v,i}$, respectively, (53) leads to

$$\boldsymbol{e}_v(t) = -k_c (\boldsymbol{L} \otimes \boldsymbol{I}_p) \int_{t_0}^{t} \boldsymbol{e}_v \, d\tau - \tilde{\boldsymbol{x}}_v \tag{54}$$

in which, from (40), $\tilde{\boldsymbol{x}}_v$ converges to the origin in finite-time. Finally, since the communication graph is connected, the immediate consequence of (54) is that $\int_{t_0}^{t} \boldsymbol{e}_{v,i} = \int_{t_0}^{t} \boldsymbol{e}_{v,j}$, $\forall\, i, j$ which, based on (42) and (52), implies that $\boldsymbol{e}_{v,i} = \boldsymbol{0}_p$ $\forall\, i$. This completes the proof.

References

1. B. Lacevic, P. Rocco, and A. M. Zanchettin. Safety assessment and control of robotic manipulators using danger field. *IEEE Trans. Robot.*, 29(5):1257–1270, 2013.
2. M. Lippi and A. Marino. Safety in human-multi robot collaborative scenarios: a trajectory scaling approach. *IFAC-PapersOnLine*, 51(22):190 – 196, 2018.
3. D. P. Losey, C. G. McDonald, E. Battaglia, and M. K. O'Malley. A review of intent detection, arbitration, and communication aspects of shared control for physical human–robot interaction. *Applied Mechanics Reviews*, 70(1):010804, 2018.
4. S. Musić and S. Hirche. Control sharing in human-robot team interaction. *Annual Reviews in Control*, 44:342 – 354, 2017.
5. C. Masone, M. Mohammadi, P. Robuffo Giordano, and A. Franchi. Shared planning and control for mobile robots with integral haptic feedback. *Int. J. Robot. Res.*, 37(11):1395–1420, 2018.
6. Y. Li, K. P. Tee, W. L. Chan, R. Yan, Y. Chua, and D. K. Limbu. Continuous role adaptation for human–robot shared control. *IEEE Trans. Robot.*, 31(3):672–681, June 2015.
7. D. P. Losey and M. K. O'Malley. Trajectory deformations from physical human–robot interaction. *IEEE Trans. Robot.*, 34(1):126–138, Feb 2018.
8. A. Mörtl, M. Lawitzky, A. Kucukyilmaz, M. Sezgin, C. Basdogan, and S. Hirche. The role of roles: Physical cooperation between humans and robots. *Int. J. Robot. Res.*, 31(13):1656–1674, 2012.
9. J. R. Medina, T. Lorenz, and S. Hirche. Synthesizing anticipatory haptic assistance considering human behavior uncertainty. *IEEE Trans. Robot.*, 31(1):180–190, Feb 2015.
10. Valeria Villani, Fabio Pini, Francesco Leali, and Cristian Secchi. Survey on human–robot collaboration in industrial settings: Safety, intuitive interfaces and applications. *Mechatronics*, 55:248 – 266, 2018.
11. M. Lippi, A. Marino, and S. Chiaverini. A distributed approach to human multi-robot physical interaction. In *IEEE Int. Conf. on Systems, Man and Cybernetics*, pages 728–734, 2019.
12. O. Khatib. A unified approach for motion and force control of robot manipulators: The operational space formulation. *IEEE J. Robot. Autom.*, 3(1):43–53, 1987.
13. R. Colbaugh, H. Seraji, and K. Glass. Direct adaptive impedance control of robot manipulators. *J. Robot. Syst.*, 10(2):217–248, 1993.
14. Md. M. Rahman, R. Ikeura, and K. Mizutani. Investigation of the impedance characteristic of human arm for development of robots to cooperate with humans. *JSME Int. J. Series C Mechanical Syst., Machine Elem. and Manufacturing*, 45(2):510–518, 2002.
15. Etienne Burdet, David W Franklin, and Theodore E Milner. *Human robotics: neuromechanics and motor control*. MIT press, 2013.
16. T. Tsumugiwa, R. Yokogawa, and K. Hara. Variable impedance control based on estimation of human arm stiffness for human-robot cooperative calligraphic task. In *IEEE Int. Conf. Robot. Autom.*, volume 1, pages 644–650 vol.1, 2002.
17. Y. Li and S. S. Ge. Human–robot collaboration based on motion intention estimation. *IEEE/ASME Trans. Mechatronics*, 19(3):1007–1014, 2014.
18. M. S. Erden and A. Billard. Hand impedance measurements during interactive manual welding with a robot. *IEEE Trans. Robot.*, 31(1):168–179, 2015.
19. P. K. Artemiadis, P. T. Katsiaris, M. V. Liarokapis, and K. J. Kyriakopoulos. Human arm impedance: Characterization and modeling in 3d space. In *IEEE/RSJ Int. Conf. on Intelligent Robots and Systems*, pages 3103–3108, 2010.
20. H. Modares, I. Ranatunga, F. L. Lewis, and D. O. Popa. Optimized assistive human–robot interaction using reinforcement learning. *IEEE Trans. Cybern.*, 46(3):655–667, 2016.
21. A. Marino. Distributed adaptive control of networked cooperative mobile manipulators. *IEEE Trans. Control Syst. Technol.*, 26(5):1646–1660, 2018.
22. A. Marino and F. Pierri. A two stage approach for distributed cooperative manipulation of an unknown object without explicit communication and unknown number of robots. *Rob. Auton. Syst.*, 103:122 – 133, 2018.

23. M. Mesbahi and M. Egerstedt. *Graph theoretic methods in multiagent networks*. Princeton University Press, 2010.
24. M. Selvaggio, F. Abi-Farraj, C. Pacchierotti, P. R. Giordano, and B. Siciliano. Haptic-based shared-control methods for a dual-arm system. *IEEE Robot. Autom. Lett.*, 3(4):4249–4256, Oct 2018.
25. T. Yoshikawa and X. Zheng. Coordinated dynamic hybrid position/force control for multiple robot manipulators handling one constrained object. *Int. J. Robot. Res.*, 12(3):219–230, 1993.
26. A. De Luca and R. Mattone. Sensorless robot collision detection and hybrid force/motion control. In *IEEE Int. Conf. Robot. Autom.*, pages 999–1004, 2005.
27. S. Haykin. *Adaptive Filter Theory*. Prentice-Hall, Inc., 1996.
28. O. P. Malik, G. S. Hope, and S. J. Cheng. Some issues on the practical use of recursive least squares identification in self-tuning control. *Int. J. Control*, 53(5):1021–1033, 1991.
29. N. Rao Sripada and D. Grant Fisher. Improved least squares identification. *Int. J. Control*, 46(6):1889–1913, 1987.
30. A. Bhole, F. Ficuciello, A. Mashayekhi, S. Strano, M. Terzo, L. Villani, and B. Siciliano. Online estimation of impedance parameters for a variable impedance controlled robotic manipulator. In *Advances in Italian Mechanism Science*, pages 267–274. Springer International Publishing, 2019.
31. Frank L Lewis, Draguna Vrabie, and Vassilis L Syrmos. *Optimal control*. John Wiley & Sons, 2012.
32. F. Chen, Y. Cao, and W. Ren. Distributed average tracking of multiple time-varying reference signals with bounded derivatives. *IEEE Trans. Autom. Control*, 57(12):3169–3174, 2012.
33. J. Fu and J. Wang. Observer-based finite-time coordinated tracking for general linear multi-agent systems. *Automatica*, 66:231 – 237, 2016.
34. G. Golluccio, G. Gillini, A. Marino, and G. Antonelli. Robot dynamics identification: A reproducible comparison with experiments on the kinova jaco2. *IEEE Robot. Autom. Mag.*, 2020.
35. M. Lippi and A. Marino. Cooperative object transportation by multiple ground and aerial vehicles: Modeling and planning. In *IEEE Int. Conf. Robot. Autom.*, pages 1084–1090, 2018.
36. Yanan Li and Shuzhi Sam Ge. Force tracking control for motion synchronization in human-robot collaboration. *Robotica*, 34(6):1260–1281, 2016.
37. K. Sun, J. Qiu, H. R. Karimi, and H. Gao. A novel finite-time control for nonstrict feedback saturated nonlinear systems with tracking error constraint. *IEEE Trans. Systems, Man, and Cybernetics: Systems*, pages 1–12, 2019.